University of Ferrara

Department of Physics and Earth Science

Ph.D. in Physics

Development of New Techniques for Clinical Applications of Jugular Venous Pulse with Ultrasound Devices

Advisor:

Mauro Gambaccini

Student

Valentina Tavoni

Co-Advisor:

Paolo Zamboni

2015-2018 – XXXI cycle
Coord. Prof. Vincenzo Guidi – FIS/07

University of Ferrara

Department of Physics and Earth Science

Ph.D. in Physics

Development of New Techniques for Clinical Applications of Jugular Venous Pulse with Ultrasound Devices

Advisor:

Mauro Gambaccini

Student

Valentina Tavoni

Co-Advisor:

Paolo Zamboni

2015-2018 – XXXI cycle
Coord. Prof. Vincenzo Guidi – FIS/07

to Me

Michele,

and My Parents

Contents

List of Abbreviations

A-mode: Amplitude mode
AV: Atrioventricular

B-mode: Brightness mode
BMF: Blood Mimicking Fluid

CCA: Common Carotid Artery
CCSVI: Chronic Cerebrospinal Venous Insufficiency
COV: Coefficient Of Variation
CSA: Cross Sectional Area
CVC: Central Venous Catheter
CVP: Central Venous Pressure

DWT: Discrete Wavelet Transform

ECG: Electrocardiogram

FC: Cardiac Frequency
FCC: Fraction of Cardiac Cycle

HC: Healthy Control

ID: Identification number
IJV: Internal Jugular Vein
ISB: Intrinsic Spectral Broadening

JVP: Jugular Venous Pulse

M-mode: Motion mode
MCI: Mild Cognitive Impairment
MSD: Multigate Spectral Doppler
MTD: Mean Time Delay

PCA: Principal Component Analysis
PRF: Pulse Repetition Frequency

RAP: Right Atrial Pressure
ROC: Receiver Operating Characteristic
ROI: Region Of Interest

SA: Sinoatrial
SD: Standard Deviation
SdNR: Signal difference to Noise Ratio
SV: Sample Volume
SVC: Superior Vena Cava

TAV: Time Average Velocity
TX-RX: Transmission Reception

ULA-OP: Ultrasound Advanced Open Platform
US: Ultrasound
USJD: Ultrasound Jugular Diagram

VA: Vertebral Artery

Abstract

It is recognized that internal jugular veins are the major route of cerebral outflow in supine position, and that reduced functionality of these veins can lead to neurological diseases. One of the most interesting parameters to study the functionality of these veins is the Jugular Venous Pulse (JVP) trace. JVP is useful not only to investigate drainage functions, but also to evaluate cardiac hemodynamic and to estimate Central Venous Pressure (CVP) in an indirect way. CVP is an invasive measure of blood pressure in veins close to the right atrium of the heart, that contains information about the functionality of the heart.

In recent years, my research group demonstrated that it is possible to obtain the JVP trace with Ultrasound (US) imaging. Moreover, we implemented a custom script to obtain the trace in a semi-automatic way, using a software for image processing. In this way we were able to obtain a JVP trace, by recognizing and measuring the changes of Cross Sectional Area (CSA) of the vein over time. Therefore the group focused on the correlation between CVP and JVP, in order to find a model to assess pressure variations from CSA measurements.

Part of my thesis work was dedicated to check, for the first time, the robustness of this model through an experimental validation. Another part of the thesis investigated the statistical differences between hemodynamic parameters of a group of healthy subjects and a group of patient with mild cognitive impairment. Both the projects were divided in: collection of data, traces elaboration and statistical analysis.

During the first project, we verified both the correlation and the time lag between JVP and CVP traces. Then we analysed the model for the calculation of the CVP. The achieved results were currently weak but promising. Regarding the comparison between healthy control and

pathological subjects, we found several statistical differences between the two groups. However, the results could be affected by a bias due to different age intervals of the volunteers.

In the last part of my thesis work the performances of a new US Advanced Open Platform (ULA-OP) were characterized through the comparison with a standard US device. We analysed both Doppler and Brightness (B-mode) modalities. Results showed that in Doppler mode the ULA-OP system is more accurate and less precise than the standard one. In B-mode the performances were very similar, even if the image quality was worse. However, the high programmability of ULA-OP, one of the main innovations of this device, could compensate the defects. Once implemented the necessaries adjustments, this platform could become very useful for cardiovascular diagnostics.

Abstract

E' ormai noto che le vene giugulari interne sono la via principale attraverso cui il sangue defluisce dal cervello quando si è in posizione supina e che un ridotto drenaggio cerebrale può portare a disfunzioni neurologiche. Uno dei parametri principali per studiare la funzionalità di queste vene è il polso venoso giugulare (JVP), un tracciato utile anche per valutare l'emodinamica cardiaca e per stimare in modo indiretto la pressione venosa centrale (CVP). Quest'ultima è una misura invasiva di pressione rilevata generalmente in vena cava, in prossimità dell'atrio destro del cuore: tale parametro fornisce importanti informazioni riguardo alla funzionalità cardiaca. Negli ultimi anni il mio gruppo di ricerca ha dimostrato come sia possibile ottenere un tracciato JVP da un normale esame ad ultrasuoni dei vasi cardiaci. In particolare, si è riusciti a determinare il JVP in modo semi-automatico con un software di elaborazione immagini che rileva le variazioni nel tempo dell'area di sezione trasversale del vaso (CSA). Il gruppo ha quindi individuato un modello che correlasse i tracciati di CVP e JVP al fine di calcolare una misura di pressione grazie alla sola quantificazione dell'area. Una parte del mio lavoro è stata dedicata ad una prima validazione sperimentale del modello. Un'altra parte del lavoro ha invece previsto un confronto tra i parametri emodinamici di un gruppo di soggetti di controllo sani ed un gruppo di pazienti affetti da patologie cognitive ad uno stadio iniziale. Entrambi i progetti, sviluppati in parallelo, hanno previsto una parte di raccolta dati, elaborazione dei tracciati e analisi statistica.

Durante il primo progetto è stata verificata sia la correlazione tra i tracciati JVP e CVP, sia il ritardo temporale tra gli stessi. Successivamente, è stata effettuata l'analisi del modello per il calcolo della pressione con risultati complessivamente deboli ma promettenti. Il confronto tra soggetti sani e patologici del secondo progetto ha individuato caratteristiche statisti-

camente differenti tra le due popolazioni. Tuttavia, i risultati del confronto sembrano essere influenzati dalla diversa età dei soggetti esaminati, che potrebbe modificare i parametri misurati.

Infine, il mio lavoro di tesi si è concluso con la caratterizzazione di una nuova piattaforma ad ultrasuoni (ULA-OP), effettuata tramite il confronto delle sue prestazioni con quelle di un ecografo tradizionale. Le modalità esaminate sono state due: Doppler e Brightness (B-mode). In modalità Doppler la piattaforma ULA-OP presenta una migliore accuratezza nelle misure, ma non altrettanta precisione. Invece, in modalità B-mode non si sono verificate importanti differenze rispetto alle prestazioni dell'ecografo tradizionale se non per la qualità dell'immagine, più scarsa nel nuovo dispositivo. Tuttavia, una delle grandi innovazioni di questo strumento è la possibilità di personalizzare e perfezionare il software di acquisizione ed elaborazione dati. Apportando quindi le necessarie migliorie il dispositivo si potrebbe rivelare molto utile nell'ambito della diagnostica vascolare.

Introduction

Ultrasound (US) imaging is becoming important in clinical environment, particularly in medical diagnostics. This technology allows non invasive, cheap and safe examinations, since US presents no real risk to the patient. Such technology is used also in cardiovascular diagnostics field. For example in 2008, using US imaging, Professor Paolo Zamboni and his group of the University of Ferrara discovered the Chornic Cerebrospinal Venous Insufficiency (CCSVI): a vascular condition characterised by anomalies of the main extra-cranial cerebrospinal veins [1]. Innovation research on US methodologies and devices led to a collaboration between Medical Physics group and Vascular Disease Center of the University of Ferrara. One of the principal aims of this collaboration was to improve the precision and accuracy in quantifying blood velocity and Cross Sectional Area (CSA) of the Internal Jugular Vein (IJV). Since 2013 several papers were published about new US models to calculate the amount of blood flowing from the brain [2–5]. During the last years the group implemented a new method to calculate the changes in IJV CSA with a semi-automatic tracing algorithm [6, 7]. By recording and analysing a morphological US video-clip of few seconds, it is possible to obtain a trace equivalent to the Jugular Venous Pulse (JVP). The importance of JVP is known since the beginnings of the twentieth century [8]. It is used both to investigate drainage functions of the IJVs and to evaluate cardiac hemodynamics and characteristic wave patterns that could be manifestations of cardiac diseases. Moreover, JVP is an indirect way to estimate the Central Venous Pressure (CVP), that is the blood pressure in the veins close to the right atrium of the heart. This important parameter contains information about the functionality of the heart. Nowadays, it is measured with invasive methods, using a Central Venous Catheter (CVC) inserted in a large vein of the chest.

Part of my work consisted in verifying experimentally the correlation between JVP and CVP traces measured on a group of volunteers. Moreover I applied to the measured data a model, already described in the literature [9–11], in order to quantify a predicted pressure trace using JVP values.

Another part of the work was a statistical comparison between vascular US examinations of Healthy Control (HC) subjects and Mild Cognitive Impairment (MCI) patients, since several studies demonstrate that an anomalous blood flow can be related to neurological disorders [12–16].

Finally I characterised a new US Advanced Open Platform (ULA-OP) designed by the group of Professor Piero Tortoli in 2009 [18] and already used for vascular examination [19, 20]. The characterisation consisted in comparing the ULA-OP performances with the ones of a standard device. I tested the main modalities for our vascular studies: the Brightness mode (B-mode) in-vivo, examining several volunteers, and the Doppler mode in-vitro, using a phantom with a continuous flow.

1

State of the Art

1.1 Anatomy

The circulatory system, composed by heart, vessels and blood, is one of the main organ system in the human body. It enables blood cells, oxygen and nutrients to be transported to and from the cells in the body. The circulatory system has two components, a systemic circulation and a pulmonary one. The latter lets the blood circulate through the lungs, where it gets oxygenated. The former is a loop through the rest of the body to provide fresh blood. The heart is composed by four chambers and likewise valves (Figure 1.1).

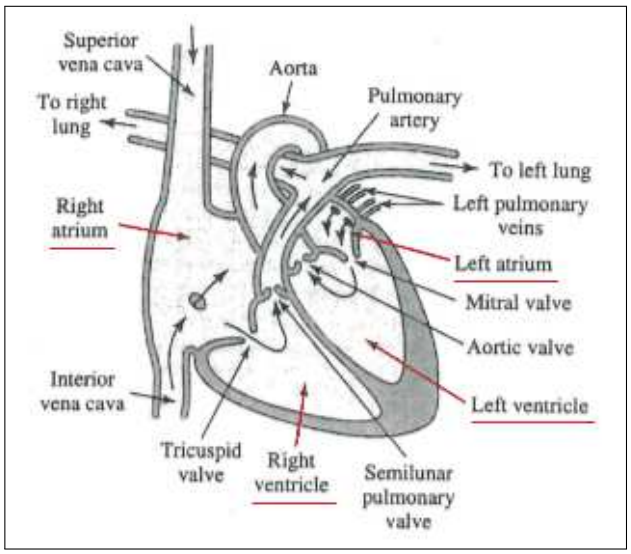

Figure 1.1: *Heart representation with its chambers and valves. Reproduced from [21].*

For each circulation, there is one atrium and one ventricle, the upper and the lower chamber respectively. The valves allows blood to flow in only one direction. They are divided in Atrioventricular (AV) and semilunar valves. AV valves, the mitral and the tricuspid one, are between atria and ventricles; semilunar valves, the aortic and the pulmonary one, are in the arteries leaving the heart. As regards the upper part of the systemic circulation (Figure 1.2), the heart pumps oxygenated blood from the left ventricle into the aorta through the semilunar valve. The aorta is the main artery in the human body, its walls are elastic and this elasticity helps maintaining the blood pressure through the body.

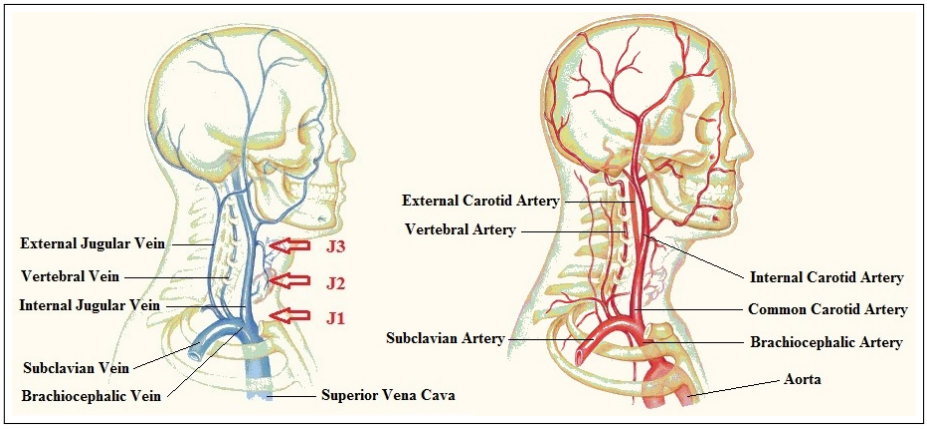

Figure 1.2: *Representation of the main arteries and veins of the upper part of the systemic circulation.*

In the upper part, the aorta makes a hairpin turn known as the aortic arch. This vessel has three branches: the first and largest branch is the brachiocephalic trunk, next comes the left common carotid artery, and finally, the left subclavian artery. The brachiocephalic trunk is divided into the right common carotid artery and the right subclavian artery. The subclavian arteries (left and right) supply blood both to arms and head with one branch on both sides. These branches are the Vertebral Arteries (VAs), which provide blood to the upper spinal cord and the posterior part of the brain. The Common Carotid Arteries (CCAs) supply head and neck with oxygenated blood. They bifurcate into the internal and external carotid arteries at around the upper border of the thyroid cartilage. The brain is nourished by the internal carotid arteries, while the external carotid arteries supply other portions of the head, such as face, skull and meninges. At this level, arteries firstly divide into small ways, called arterioles, and then into the capillaries. The capillaries join in order to bring blood into

the venous system. After their passage through body tissues, they join once again into venules, and then into veins. The IJVs are paired veins that collect blood from the brain, the outside of the face and the neck. The diameter of the IJVs range from a minimum of 0.4 cm to a maximum of 2.0 cm [22]. The elasticity of the IJVs is lower than the arterial one, as opposed to the compliance (C) [9, 11, 21, 23], defined as:

$$C = \frac{dV}{dp} \tag{1.1}$$

where dV and dp are the variations in volume and pressure, respectively. It means that the ability of the IJVs to enlarge their volume with increasing transmural pressure is greater than the arterial one. Moreover, they tend to be tortuous and present most of the time movable valves [24]. In a recent consensus, the IJV was subdivided into three segments. The upper segment, J3, is anatomically located at the carotid bifurcation, close to mandibular angle. The middle segment, J2, is approximately located at the middle of the thyroid. Finally, the lower one, J1, is located at the confluence with the brachiocephalic vein [25] (Figure: 1.2). Together with the IJVs, the external jugular veins are the jugular veins. The blood from the outside of the skull and the deep parts of the face is collected by the external jugular veins and flows into the subclavian veins. IJVs, subclavian veins and vertebral veins, flowing directly from the head, form the brachiocephalic veins, and these (left and right) merge to form the superior vena cava. It is recognized that, in supine position, the main outflow route is represented by the IJVs, while, in upright position, such outflow shifts to secondary venous channels, including the vertebral veins [2, 26]. The Superior Vena Cava (SVC) is above the heart, it is short, yet large-diameter. Therefore it is the typical site of central venous access via a CVC. SVC, together with the inferior vena cava, that receives blood from the lower part of the body, form the venae cavae. They are both situated slightly off-center, toward the right side of the body and flow into the right atrium of the heart. Blood is a non-homogeneous fluid that transports necessary substance and metabolic waste respectively to and from the cells. The amount of blood in an adult's body is roughly 5 [27, 28] litres. It is a suspension of cells in a liquid known as blood plasma. The corpuscular part, called hematocrit, makes up around 45% [29] of the whole blood and it is mainly formed by red blood cells. Blood flow in an ideal vessel is laminar, i.e. blood moves in layers that slide on each other with different velocities: slower near the vessel's walls and faster in their center. These differences determine the velocity profile (Figure: 1.3).

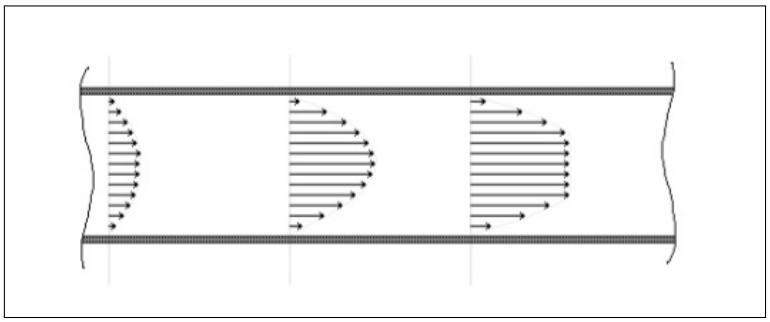

Figure 1.3: *Representation of velocity profile inside an ideal vessel.*

The velocity gradient along the diameter is due to the viscosity drag exerted by the wall, slowing the fluid. The shape of a real velocity profile is more complicated. The vessels are not perfectly straight, the blood flow is pulsating and it depends on the pressure drop along the vessels.

1.2 Cardiac Cycle

The cardiac cycle is the performance of the heart between two heartbeats. It consists of two periods: diastole and systole. During the first one, the heart muscle relaxes and refills with blood, while the second one is a period of robust contraction to pump the blood. The rate of cardiac contraction is known as the heart rate and, assuming a healthy subject in normal conditions, it is typically of 60 to 100 beats per minute [30]. Therefore, the duration of each cycle takes about 0.6-1 second. Ventricles, atria and valves work in concert to repeat the cardiac cycle incessantly. The beginning of the cycle is the ventricular diastole. The heart relaxes and expands while blood flows into both ventricles through the atria. The AV valves open to permit filling. After a short time, the atria begin to contract, atrial systole, and pump blood into the ventricles. During ventricular systole, while the atria are relaxed (atrial diastole), the ventricles are contracting and energetically ejecting two separated blood supplies both the circulations. The back-pressure against the AV valves increases and forces them to close. This phase is called isovolumic contraction. Due to contractions, the pressures in the ventricles rise quickly, exceeding the pressures in aorta and pulmonary arteries, causing the opening of the semilunar valves and blood ejection from the ventricles: ejection stage. The next step is the isovolumic relaxation, during which the pressure within the ventricles begins to fall

significantly, both the semilunar valves close and the AV valves open again, and consequently the heart begins to refill.

Every step in the cardiac cycle is regulated by electric stimulations known as action potentials. The heart has a center that generates rhythmic electric signals, which are conducted to every muscle cell. This center is called Sinoatrial (SA) node and is located in the wall of the right atrium of the heart, near the entrance of the superior vena cava. It is composed by pacemaker cells, that create the periodic impulses. The main role of the SA node is to initiate an action potential that passes throughout the heart and causes its contraction. An action potential is a change in voltage across the cell membrane, produced by ion movements, and is composed by two phases: first the depolarisation and next the repolarization. Non-pacemaker cells have a period between the repolarization and the depolarisation, where the membrane potential remains quite constant. This resting phase ends when another impulse arrives to the cell. Pacemaker cells are not subjected to any resting phase. Immediately after an action potential, the membrane potential begins to depolarise again. Once it reaches a threshold value, a new action potential is produced and so on. The cardiac electric signal spreads radially from the SA node throughout the right atrium, until the left atrium and the AV node. The AV node is the part of the electrical conduction system joining atria and ventricles and coordinating the top of the heart. The AV node is located at the lower back section of the wall that separates the two atria. When the signal from the SA node reaches the AV node, it is delayed for a given period of time in order to allow the ventricular filling during atrial systole.

The electrical activity of the heart can be recorded with a technique called Electrocardiogram (ECG). The signal is measured using electrodes, placed on the skin of the subject, that detect the tiny electrical changes due to polarization and depolarization of the cells.

To better understand the relation between mechanical and electric events during a heartbeat, a plot with the most significant traces is here reported (Figure 1.4) [21, 31].

ECG trace shows the P wave distinctive of atrial depolarization, the QRS complex induced both by ventricular depolarization and atrial repolarization, and the T wave representing ventricular repolarization. Left ventricle and aortic pressure curve are represented in the upper part of the figure. When the left ventricle pressure exceeds the pressure in the aorta, the aortic valve opens and blood is ejected into the aorta. In the moment when the valve closes, the ventricular pressure is smaller than

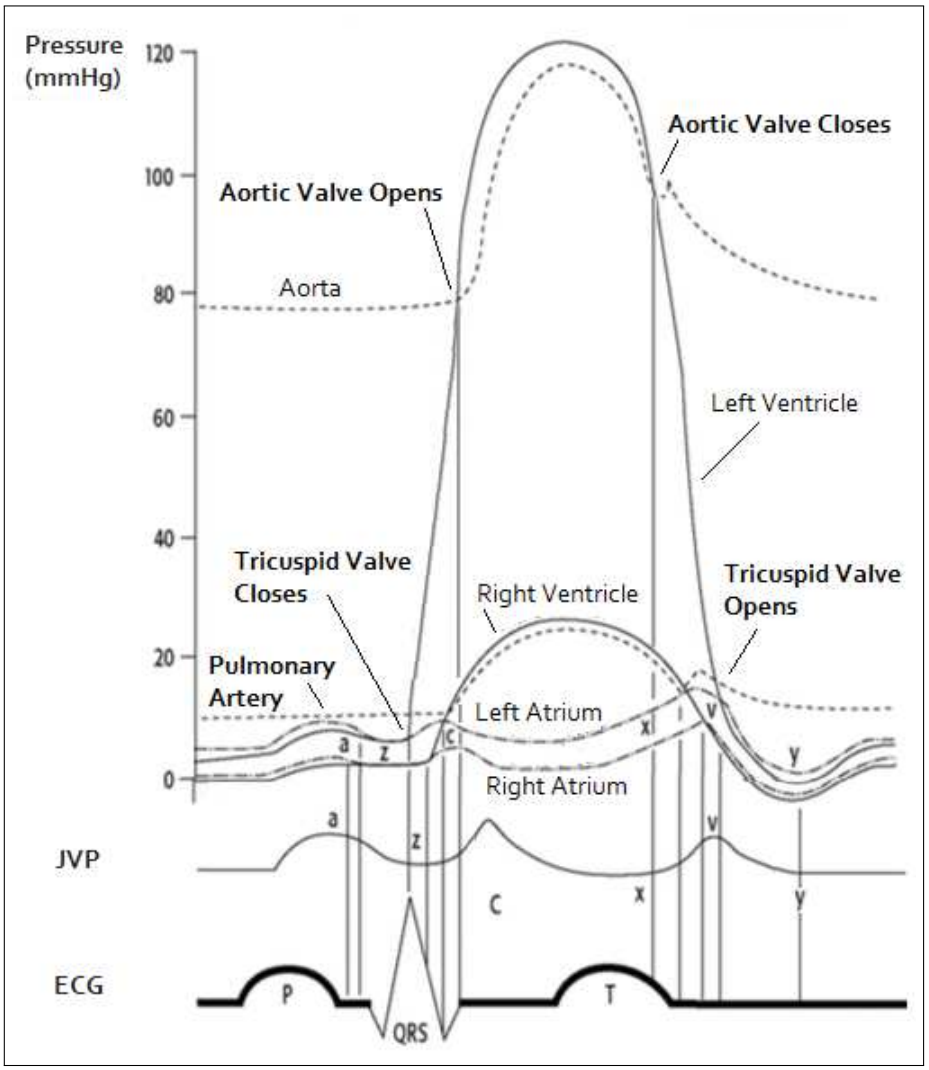

Figure 1.4: *Representation of the main traces of mechanical and electrical events. Electrocardiogram (ECG), Jugular Venous Pulse (JVP) and Pressure curves of Aorta, Left and Right Ventricle, Pulmonary Artery, Left and Right Atria.*

the aortic one and the ejecting jet decelerates until it stops. The Right Ventricular pressure curve is similar to the left ventricle's one, though at a lower level. JVP represents the movements of the IJV. The trace shows an a wave due to right atrial contraction at end diastole. The c wave reflects the backward movement of the tricuspid valve to the right atrium during ventricular systole. The x wave represents the downward displacement of the base of the ventricles during systole and continued atrial relaxation. The v wave is due to the filling of the right atrium. The y wave follows

the opening of the tricuspid valve. The Right Atrial Pressure (RAP) wave, often almost identical to CVP [32], is essentially the same as the JVP. Left Atrial pressure curve is similar to the right atrium's one.

1.3 CVP and JVP traces

CVP is the blood pressure in the veins close to the right atrium of the heart. This parameter contains information about the amount of blood returning to the heart and its functionality, indeed there is a reciprocal relation between measurements of CVP and the function of the heart, for example an elevated venous pressure is an early and essential finding of heart failure [33, 34]. A single measurement of the CVP is able to discover whether a heart is efficient or not. Moreover, repeated observations over a period of time are an excellent measure of its health state [35]. CVP can be measured directly by using a CVC inserted in a large vein of the neck or the chest. (Figure 1.5)

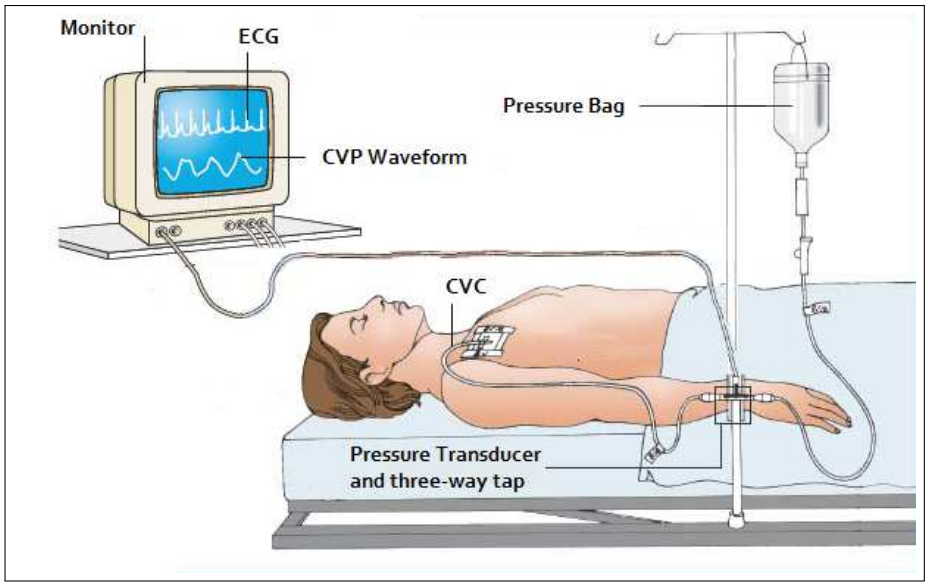

Figure 1.5: *Representation of a measurement session of central venous pressure via central venous catheter.*

The catheter of the subject is connected to a specific infusion set, which is connected to a transducer. Once the system is properly calibrated, the device transmits the CVP signal to a monitor. This procedure is quite complicated, it is invasive and needs a surgical operation in order to

insert the CVC. Moreover, the insertion may cause several complications. Some of these may occur during the CVC placement, for example damages to central veins, lung-related complications or cardiac problems such as abnormal heart rhythms or, although rare, cardiac arrest. Other possible complications could be directly related to the device, like breakage of the catheter itself, or due to an infection, that may consequently lead to blood poisoning, shock or even death [36–39].

An indirect way to estimate the CVP is the JVP [34, 40–42] . The JVP represents the expansion movement of the IJV as a result of pressure changes in the right atrium of the heart and over the venous system [6]. These changes proceed along the vein through mechanical waves with a specific velocity of propagation and lead to a periodic change of the IJV CSA, in accordance with the cardiac and respiratory cycle. The velocity of propagation (c) is quantified by following the Moens-Korteweg equation:

$$c = \sqrt{\frac{E}{\rho} \cdot \frac{h}{2R}} \tag{1.2}$$

where h is the vein wall thickness, ρ the blood density, R the radius of the CSA (supposed to be circular) and E the Young's modulus.
Young's Modulus for cylindrical geometry can be assumed as [23]:

$$E = \frac{2R}{h} \cdot K \tag{1.3}$$

where K is the bulk modulus defined as:

$$K = V \cdot \frac{dp}{dV} = \frac{V}{C} \tag{1.4}$$

with V volume of the vein, dp and dV variations in pressure and volume and C compliance.
Using the definition 1.1, 1.2, 1.3 and 1.4, the propagation velocity can be calculated as:

$$c = \sqrt{\frac{K}{\rho}} = \sqrt{\frac{V}{C \cdot \rho}} \, . \tag{1.5}$$

The JVP waveform present almost the same deflections of the CVP [31, 32]: its time diagram was discovered in the early 1900s and became essential for the evaluation of the central venous return to the heart [8, 43, 44]. A normal JVP waveform (Figure 1.4 and 1.6) contains 5 components: three upward deflections (a, c and v) and two downward deflections (x and y).

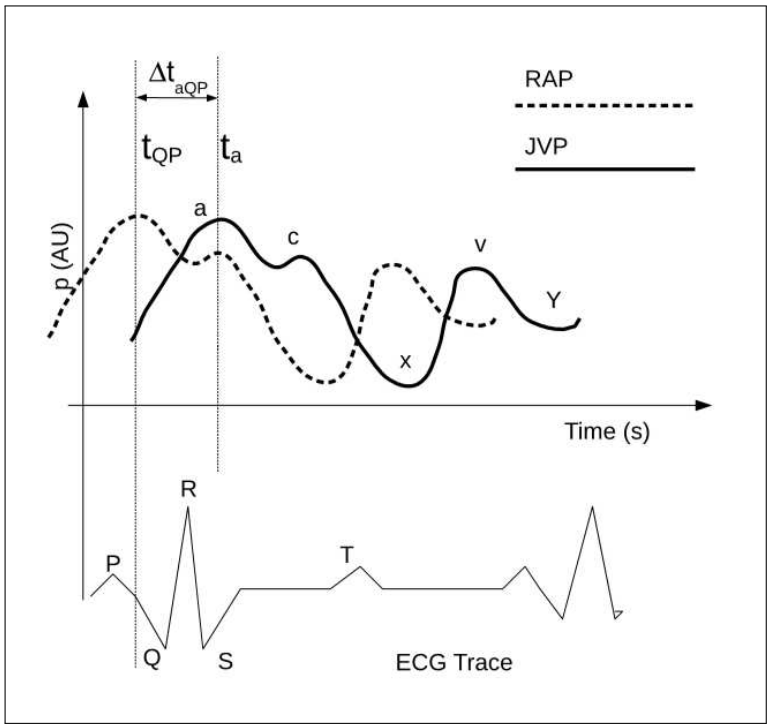

Figure 1.6: *Representation of Right Atrial Pressure (RAP), jugular venous pulse (JVP) and electrocardiogram (ECG) traces. Reproduced from [10].*

The a wave corresponds to the atrial contraction and is synchronized with the P wave of the ECG. The c wave immediately follows the R peak of the ECG and reflects ventricular contraction and resulting backward movement of the tricuspid valve to the right atrium. The first downward deflection x corresponds to the lowering of the AV valve during ventricular systole and continued atrial relaxation. The v wave is due to the venous filling of the right atrium and corresponds to the end of the T wave in the ECG. Finally, the y descent corresponds to the opening of the tricuspid valve and the filling of the ventricle. For the sake of completeness, it is worth mentioning that, when the diastole is long, the descending limb of the y wave is often followed by a small, positive wave (referred to as the h wave) which occurs just prior to the next a wave [45]. It is worth noting that the JVP evaluation gives useful information not only about the CVP, but also related to cardiac hemodynamics and characteristic wave patterns that could be manifestations of cardiac diseases. For these reasons, the JVP assessment may be important for managing many emergency conditions, as well as in diagnosis, monitor and prognosis of several heart

diseases [6]. Furthermore, the JVP is useful in order to investigate the drainage function of the IJVs: a poor or anomalous blood flow can be related to brain drainage problems, such as delayed venous return [46], or even to some neurological disorders [1, 12–17].

The instrument used to evaluate the JVP in the last century was the polygraph (Figure 1.7).

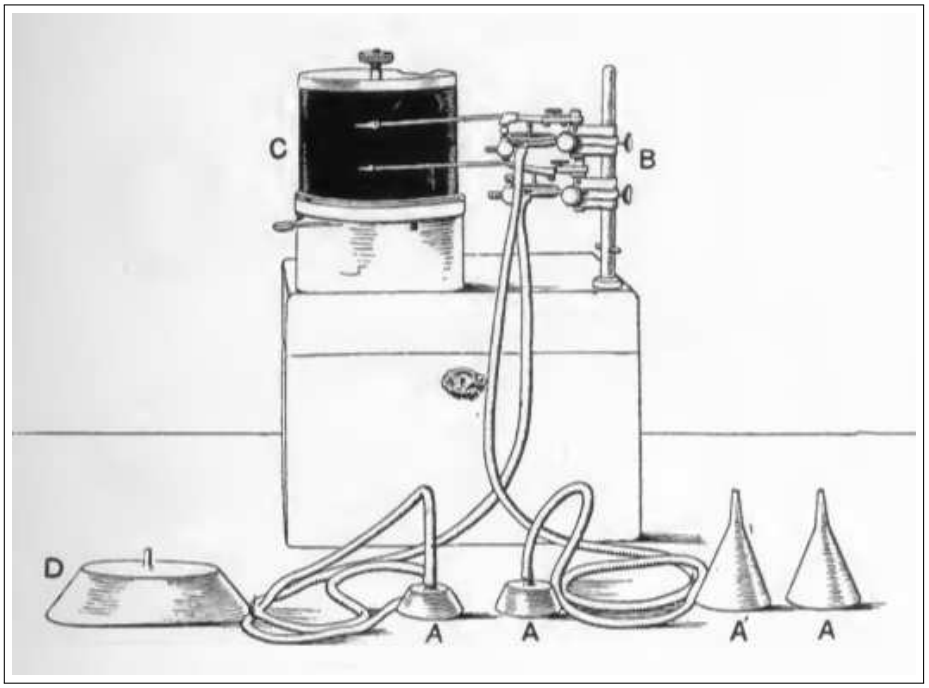

Figure 1.7: *Representation of a polygraph: the receivers, the levers and a revolving drum covered by smoked paper. Reproduced from [8].*

Such apparatus could be employed for measuring carotid pulse, venous pulse and also respiratory movements, simultaneously and on the same recording surface. The instrument was composed by a small cup for receiving the pulsations, a tube for transmitting the signals to a tambour and a lever. The tambour was connected to a sphygmograph, a device composed by a levers system fixed to a scale, useful to determine the amount of external pressure needed to stop the blood flow [8]. Either a microphone or a motion sensor are currently used in non-invasive techniques for recording the JVP trace. Thanks to these methods, pressure changes are only qualitatively represented [7]. Despite the general consensus that JVP assessment is desirable [47–50], nowadays it is often overlooked: this happens because the current way to evaluate the JVP is highly conditioned

by the individual skills of the clinicians [6]. In order to overcome these issue, during the last years a new method has been demonstrated as a way to deduce both a qualitative and quantitative JVP trace: acquiring a morphological video of the movements of the CSA with the US technology [6, 7, 51]. It is known that transmural pressure (i.e. the difference between internal and external pressure) and IJV CSA, when the vein has not collapsed, are correlated [31]. This correlation is expressed thanks to the compliance parameter. As previously defined, Volumetric Compliance is: (1.1) $C = dV/dp$, where dV and dp are the changes respectively in volume and pressure. However, the volume variations of a vessel are given only by CSA changes, hence it is possible to express dV in terms of constant length (l) and area variations ($dCSA$):

$$dV = l \cdot dCSA \tag{1.6}$$

at this point, a 2D compliance C', or compliance for unit of length, can be defined as a ratio between area and pressure variations:

$$C' = \frac{C}{l} = \frac{dCSA}{dp} \, . \tag{1.7}$$

Therefore, it is possible to describe the function of the internal pressure $p(t)$, assumed to be linearly related to the $CSA(t)$, as follows [9, 31, 52, 53]:

$$p(t) = p_0 + \frac{1}{C'} \cdot CSA(t) \tag{1.8}$$

where p_0 is a convenient additive constant. It demonstrates that is possible to represent the JVP trace with a time diagram of CSA which reflects the changes in pressure [9]. The importance of the improvement from a qualitative to a quantitative JVP trace had already emerged in the past, when a calibrated JVP was used [54]. Moreover, this technique goes beyond the limit of calibration and allows to measure numeric parameters from the trace, that can be used for clinical evaluations [7]. As previously described, in order to obtain a JVP trace it is necessary to record a video clip of a few seconds of the IJV CSA [6]. B-mode facilitates the display of the area and its variations during cardiac cycle. CSA is measured in each frame of the video clip: the collected data set represents the JVP trace. Moreover, acquiring the IJV video clip together with the ECG trace allows to identify the relationship between the two traces and to scale the time in Fractions of Cardiac Cycle (FCC) [7].

1.4 US Technology

Nowadays in clinical environment, particularly in medical diagnostics, the US technology is becoming very appealing. In most cases, US imaging is the first line of investigation before alternative imaging techniques. Differently from other methods, this one presents no real risk for the patient and allows to do non-invasive, cheap and safe examinations. Such technology is also used in cardiovascular field, since blood interacts with US beam thanks to the red blood cells [5, 55, 56]. The simplest US modes are B, M (Motion) and A (Amplitude) (Figure: 1.8).

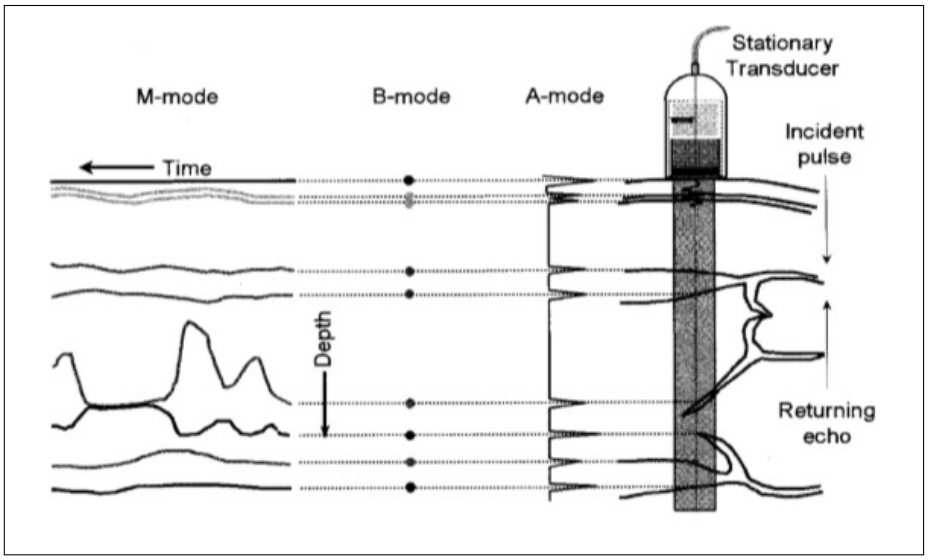

Figure 1.8: *Representation of US modes.*

The B-mode image is a morphological representation of tissues and organ boundaries inside the body (See section *1.4.3*). The M-mode shows the motion of tissues, whereas the A-mode image shows the amplitude of the received echoes. Moreover, it is possible to take advantage of the Doppler effect in order to observe the movement of blood and tissues inside the body (See section *1.4.3*). Several display modes are available also in this case: Spectral Doppler, which plots Doppler frequency shift versus time, and the Colour Flow, that shows a colour-coded for blood motion and superimposes it on the B-mode image.

1.4.1 US and Sound Waves

US are sound waves with frequencies above 20 kHz, higher than the audible limit of human hearing. These waves are longitudinal and mechanical, so

they propagate through a medium. The particles of the medium oscillate producing regions of compression and rarefaction. This excitation and its associated energy are transported by the wave. The rate at which a source of sounds produces energy is stated by its power, whereas the intensity is defined as the power flowing through the unit area perpendicular to the direction of propagation (Figure: 1.9).

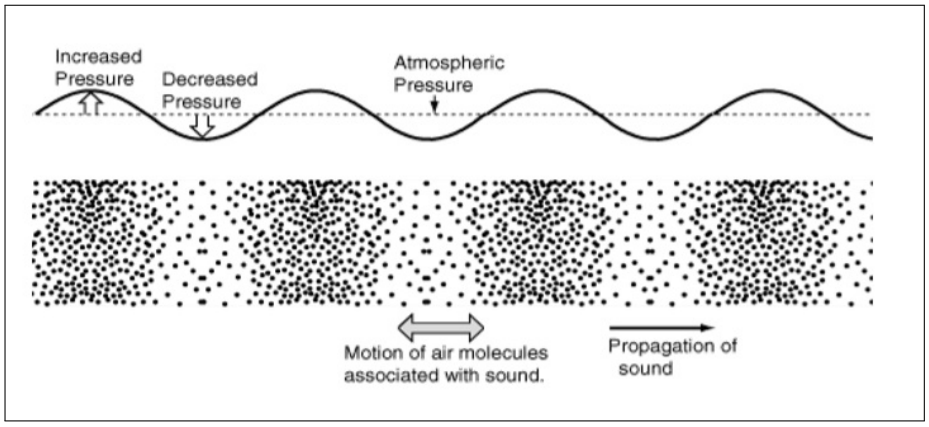

Figure 1.9: *Representation of sound waves propagation.*

The main features of waves are amplitude, frequency, wavelength and velocity. The amplitude is the maximum displacement of a particle of the medium from its equilibrium position. The frequency (f) is the reciprocal of the period and represents the number of oscillations received by a stationary observer per unit of time. The frequency of medical diagnostics US is in the range 2-15 MHz. The wavelength (λ) is the distance between consecutive wave crests. The relation between wavelength and frequency is defined as:

$$c = f\lambda \tag{1.9}$$

where c is the propagation velocity of the wave, in this case the speed of sound. In human soft tissues this velocity is rather similar: an average value of 1540 m/s can be assumed [57].

US imaging is produced from echoes, which are generated by the reflection of waves at tissue boundaries between two materials with different acoustic impedance. Acoustic impedance (z) represents the response of the particles of a medium to the passage of a wave and is defined as:

$$z = \rho c \tag{1.10}$$

where ρ is the density of the medium.

When a wave, travelling through a certain kind of tissue, hits an interface, part of the wave's energy is reflected and scattered producing echoes. The remaining part is transmitted. Some of the echoes travel back to the source and are detected by the probe that emitted the wave. In soft tissues, reflection is less than 1% for most of the interfaces. The remaining wave is transmitted and can produce echoes at deeper interfaces; the presence of air, instead, produces a reflection of 99.9% [57]. In case of non-normal incidence or different speeds of sound between two materials, the direction of propagation of the wave changes as it crosses the boundary, an effect known as refraction. The beam is also subject to US attenuation, the loss of acoustic energy by distance travelled: when a wave propagates through a medium, its particles absorb part of the energy. The result is an exponential decrease of the beam intensity as a function of the thickness (x) of the material:

$$I(x) = I_0 e^{-\mu x} \tag{1.11}$$

where I_0 is the initial intensity and μ is the linear attenuation coefficient. The μ value depends on the material and it is proportional to the beam frequency, hence for the imaging of large or deep organs a low frequency is preferred (Figure: 1.10).

1.4.2 US Devices

The device for diagnostic US imaging consists of several parts: the probe, that emits and receives US waves, the US scanner with its processor and other dedicated elements, which processes and displays the signal, and finally the software, which allows to record, modify and analyse the images. (Figure 1.11)

Hardware

The US probe is the tool that performs the examination [57]. It allows to send and receive ultrasonic signals, converting electrical energy into US pulses and conversely echoes into electrical signals. According to the target of the analysis, several types of probes are available. They differ in number, size, shape and arrangement of transducer elements. For example, when the region of interest extends right up to the surface a linear probe is suitable. This typically contains several tens of rectangular transducer elements. All transducers have the same basic components: a matching layer, a backing block, an acoustic absorber and a thin piezoelectric plate,

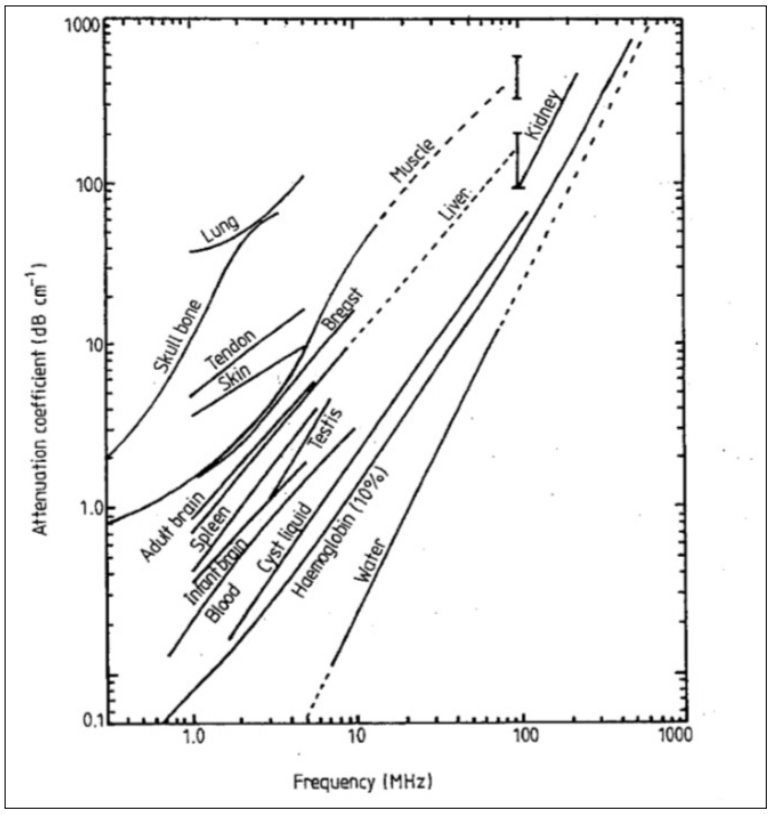

Figure 1.10: *Variation of the attenuation coefficient with frequency in different biological tissues.*

the component which generates and detects the US wave. This expands and contracts when a voltage is applied across it and, conversely, it generates a voltage when compressed or stretched by an external force. The transducers are controlled by the beamformer, this important device sends the signals in a specific direction by means of algorithms to form a wavefront that generates constructive interference. The signal produced by the echo in each transducer element must be amplified, digitalised, delayed and added to those coming from the other elements. These processes take place inside the US scanner, where the resulting signal is formed. Here, the signal is sampled, i.e. it is measured at regular intervals, to produce a sequence of numbers corresponding to the signal values. The sample rate must be at least twice the highest frequency present in the analog signal, in order to accurately reconstruct the signal and avoid aliasing. A remarkable advantage of digitalisation is that the sets of numbers, composing the signal, are immune to noise, interference and distortion.

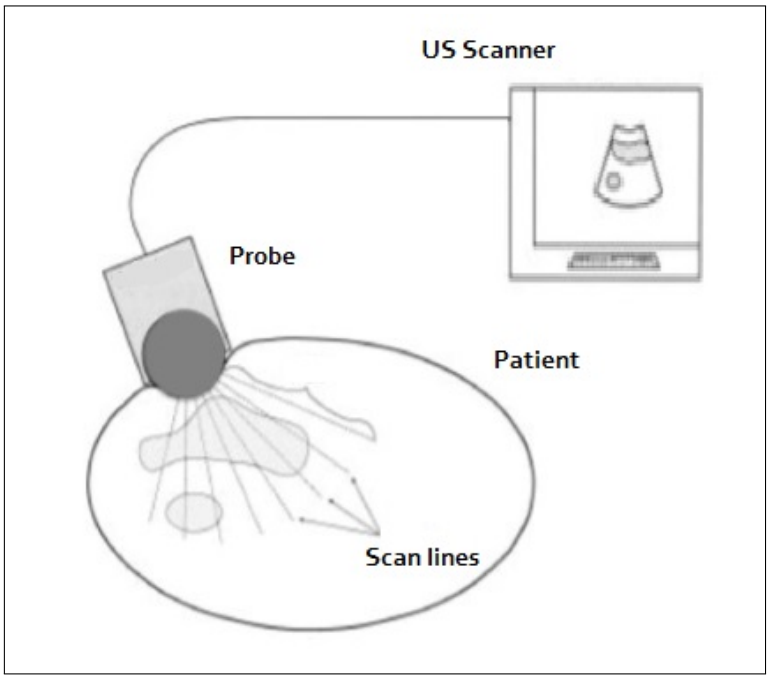

Figure 1.11: *Representation of a US device.*

Software for Image Processing

The last elements necessary to make a US examination are the software: proprietary software, customized by the same companies that build the US devices and neither accessible nor editable by the users, or open source programs (Figure: 1.12).

During the examination, the system software guarantees the best use of the device, allowing to change some settings when necessary. Moreover, it permits to view, enhance and record images. In post processing, the same software, or an equivalent one specialised in image processing, is used to analyse the stored files. The images could be modified graphically (contrast, brightness, saturation, etc.) or it is possible to measure area, length or spatial coordinates.

1.4.3 US modalities to study the circulatory system

In order to study blood flow and vessels of the circulatory system, two parameters are required: blood velocity and the CSA of the vessel. These values can be obtained with different US modes: the brightness mode for studying the variations of the area and the Doppler mode to measure the velocity of the blood.

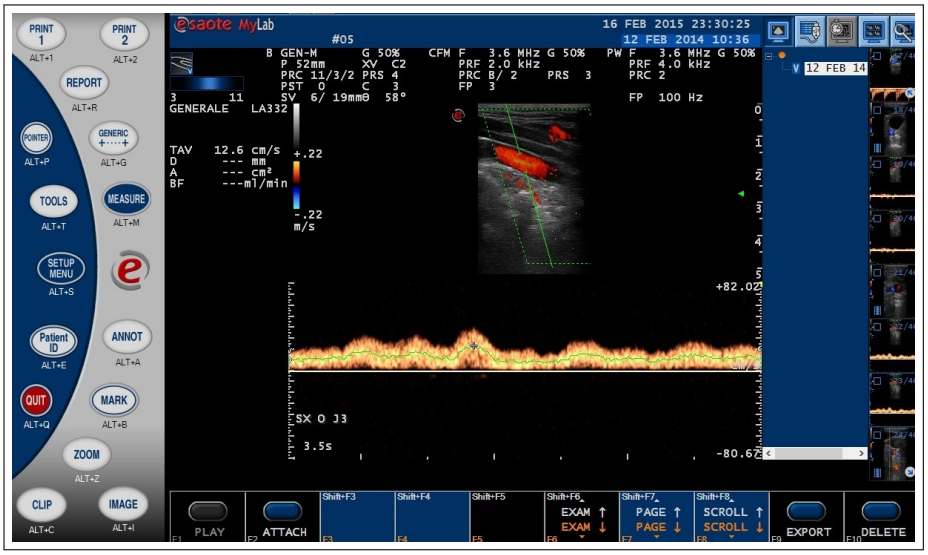

Figure 1.12: *Example of proprietary software.*

B-mode

B-mode, or brightness-mode, is a two-dimensional representation of tissues and organ boundaries inside the body. (Figure 1.13)

To produce a B-mode image of a target, the transducer sends short pulses of US and detects echoes emitted. Each echo is displayed as a point, its position corresponds to the origin of the echo-signal within the body cross section, while its brightness shows the amplitude of the echo. In order to estimate the distance from target to probe, the system has to measure the interval of time (t) between pulse transmission and echo detection. Assuming c as speed of sound in the medium, the depth (d) can be calculated as:

$$d = \frac{ct}{2} \, . \tag{1.12}$$

The 2D B-mode image is formed by a large number of lines, each of which is produced by an echo-sequence. When the pulse start, a spot begins to travel down from the top of the screen, position of the transducer, following the path of the pulse. Echoes from points near the transducer return first, whereas further echoes return later as the spot travels down the screen. A complete image is made up of 100 or more lines produced from left to right during each echo-sequence. In the unit of time a lot of frames are formed and displayed with negligible delay, therefore it is possible to consider these images as a real-time display of the inspected region.

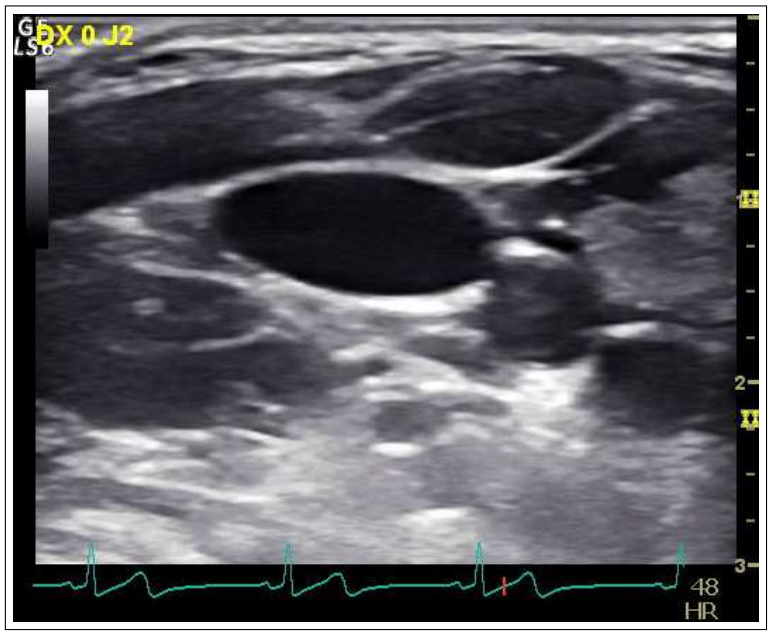

Figure 1.13: *B-mode images of a IJV CSA.*

The system makes several assumptions to form a B-mode image. Unfortunately significant variations sometimes give rise to visible image artefacts. Some examples are reported here: *the speed of sound is considered as a constant*, therefore whether the velocity of the wave changes, it can produce some mistakes such as wrong measurements of distance, distortion of interfaces or errors in size. *The beam axis is straight*: this hypothesis does not take into account the deflections due to refraction. The echoes coming from a refracted beam are shown along the scan line according to their time of arrival and so displaced from their correct location. *The attenuation in tissue is the same at any depth*: this is not correct. As said previously, pulses and returning echoes are attenuated as they propagate through tissues. This makes the echoes coming from deep targets weaker than those from similar superficial targets. Modern systems apply a constant rate of compensation in order to correct the attenuation effect, but if the value does not match the actual attenuation rate, then the inappropriate adjustment results in bright or dark bands of echoes across the image of a uniform tissue. Another source of artefacts inside the image is the reflection of the US wave due to a large smooth curved interface: those parts of the interface that are perpendicular to the incident beam give rise to strong echoes, whereas other parts with an angle of incidence greater than 10° are not shown, because the reflected beam misses the transducer.

In vascular studies the B-mode technique is used to take image of the vessels. A key role is assumed by the position of the probe: in order to obtain a cross-sectional image, the probe has to be perpendicular to the length of the vessel. On the other hand, to display the vessel in a longitudinal image, the probe has to be positioned in a way parallel to the length of the walls [58].

Doppler Mode

The Doppler effect is the variation in frequency between the reflected sound wave (f_r) and the transmitted one (f_t). It is due to the relative motion between the observer and the source. If they are moving towards each other, the wavefronts of the echoes travel closely packed and the observer perceives a frequency higher than the real one. On the contrary, if they are moving away from each other, the wavefronts are more separated and the observed frequency is lower than the transmitted one (Figure: 1.14).

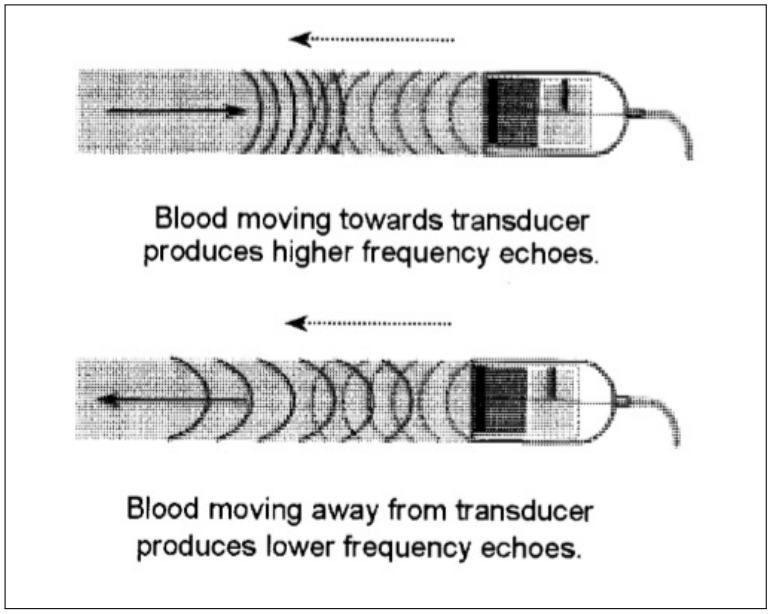

Figure 1.14: *Representation of the Doppler effect.*

In a vascular examination, the Doppler mode is used to evaluate the blood velocity by measuring the US frequency when the waves are scattered by the moving blood. The transducer is kept stationary, while the transmitted wave reaches the blood. The US frequency perceived by the red cells depends on whether the blood is stationary or is moving either to or away from the probe. The blood scatters the waves, some of which

return to the transducer and are detected: these undergo another frequency shift due to the blood movement, acting now as a source. Therefore the Doppler shift occurs twice between the US transmission and the detection. The value of the Doppler shift (f_d) depends on the transmitted frequency, the speed of sound (c), the blood velocity (v) and the angle of insonation (θ) between the beam and the direction of the blood flow:

$$f_d = f_r - f_t = \frac{2\, f_t\, v\, \cos\theta}{c}\ . \tag{1.13}$$

In order to obtain the maximum value for the Doppler shift, the vessel and the beam should be aligned, but generally the response can be considered good if the angle is less than 60° [59]. The transmitted frequency is usually of the order of few MHz, while the obtained Doppler frequency is about few kHz. By rearranging the formula, it is possible to obtain the blood velocity:

$$v = \frac{c\, f_d}{2\, f_t\, \cos\theta}\ . \tag{1.14}$$

The velocity values provided by the device are measurements assessed over the entire area (A) of the Sample Volume (SV) and spatially mediated:

$$v_m = \frac{\int_A v(a,t) n da}{\int_A da}\ . \tag{1.15}$$

Different Doppler systems can transmit and receive waves in continuous or pulsed way. In continuous systems, transmission and reception must be separated: therefore, different elements of the probe are used simultaneously and the area where the signal originated is determined by the overlap of the two beams. Differently, the most common pulsed systems, although limited in maximum frequency shift detectable, enable to receive the Doppler signal originated in a particular region, choosing depth and length of the SV.

The received signal is elaborated from the processor in order to obtain the change in frequency due to the Doppler effect. The phase-domain analysis is composed of three steps: demodulation, filtering and frequency estimation. The raw received signal is composed of the echoes generated by Doppler effect with stationary and moving tissues and blood and the transmitted signal: therefore it is necessary to isolate only the signal produced by the blood. Demodulation is the separation of low frequency components, the Doppler signal, from the high frequency components, transmitted pulse. Band-pass filtering of the signal can remove the high contribution and the lowest one, generally due to the interaction of waves

with body tissues. Finally, it is possible to obtain information concerning blood velocity with a frequency estimation: an analyser calculates the amplitude of all the frequencies present within the Doppler signal using the Fast Fourier transform method. A high production rate of spectra ensures to get quickly a detailed updating of the velocity range in the sample.

It is worth noting that the Doppler shift can be determined by the signal, provided that there are a sufficient number of pulses per period, otherwise a phenomenon called aliasing occurs. If the Pulse Repetition Frequency (PRF), that is the pulses number of a repeating signal in a specific time unit, is too low, the number of samples is not sufficient to accurately detect the Doppler frequency. The minimum limit is equal to two samples per cycle and it is known as Nyquist limit. This condition is equivalent to saying that the maximum shift detectable is equal to half the PRF (Figure: 1.15).

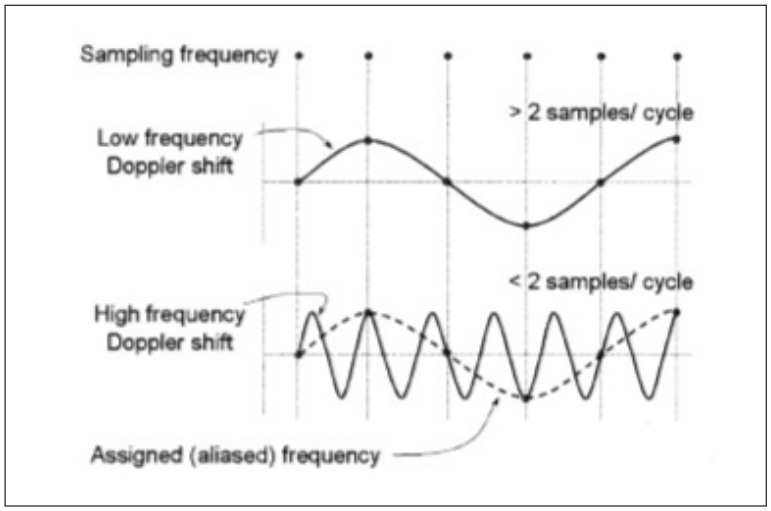

Figure 1.15: *Representation of an accurately detected frequency and aliasing.*

The main display modes for the Doppler signals are the Spectral Doppler and the Colour Flow Imaging. In the Colour Flow Imaging, the blood motion is colour coded and superimposed on the B-mode image (Figure: 1.16). The colour indicates either the presence or the absence of moving blood, and includes also a codification for the motion towards the probe or in the opposite direction.

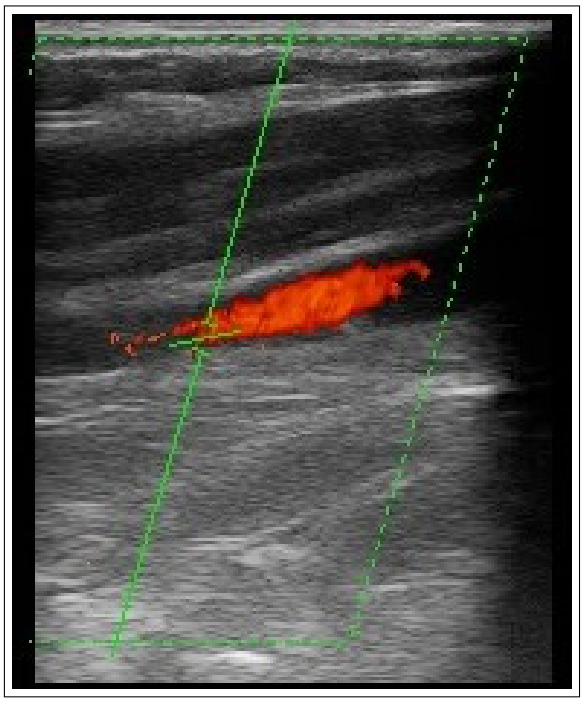

Figure 1.16: *Colour Flow image of a blood flow.*

In the Spectral Doppler, the information about velocities is shown in a plot of frequency shift against time. The height of a point is its Doppler shift, whereas the grey scale represents its amplitude (Figure: 1.17 and 1.18). The spectrum includes information regarding velocity and direction of the flow in addition to the degree of pulsatility. The range of frequencies within the spectrum is due to the velocity variation of the blood flow. With the angle of insonation it is possible to convert the frequency scale into the velocity one. Many settings can be adjusted in order to optimise the trace. The transmitted power can be intensified, so that echo signals result higher in amplitude, at the price of an increased patient exposure to US. The signal produced by blood is amplified, because it is too low to be analysed. By rising the gain, the brightness of the spectrum increases. However, if the gain is set too high, it gives rise to an artefact through which a mirror image appears in the trace. The transmitted frequency can be modified according to the depth of the vessel, if the signal is too low it is necessary to reduce the frequency for increasing the US penetration. The PRF has both a lower and an upper limit: if it is too low, aliasing may occur, but at the same time it cannot be so high to let more than a pulse in flight at once, in order to avoid confusion between the returning signals.

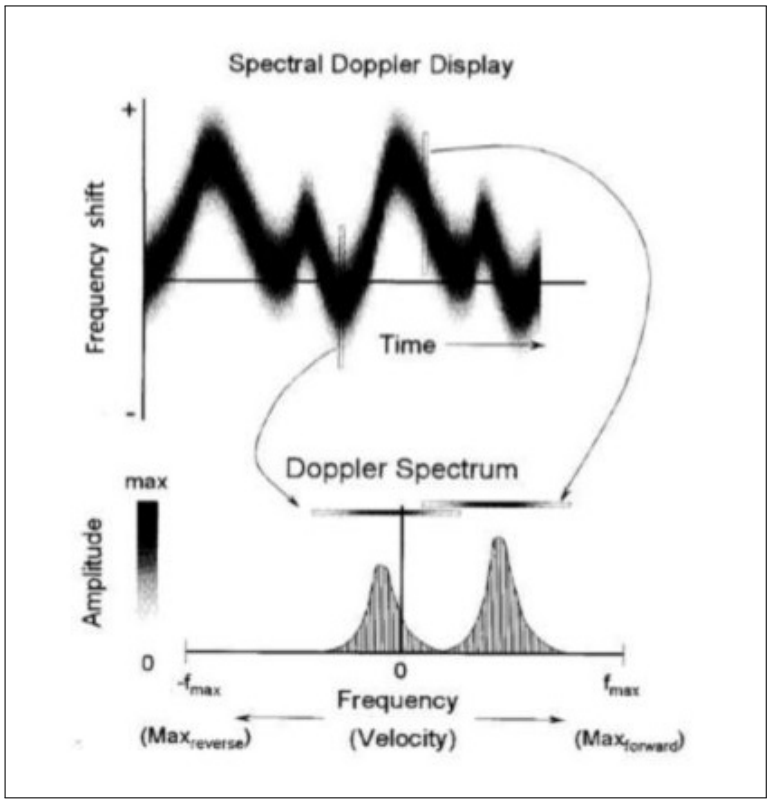

Figure 1.17: *Representation of a Spectral Doppler trace.*

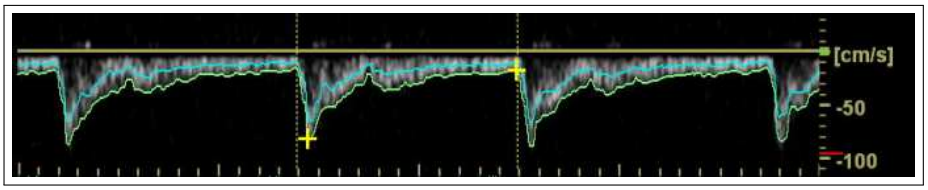

Figure 1.18: *Spectral Doppler trace.*

It is possible to combine B-mode and Doppler mode at the same time in the so called Duplex scanning (Figure 1.19), and also the Colour Flow Imaging in Triplex scanning (Figure: 1.12). They allow both a location of the SV, and an estimation of the angle of insonation, in real time during Doppler measurements.

1.4.4 Image Properties - Quality Control Test

The performance of an US system can be characterised in terms of image properties; these can be measured with specific tests [60] (Figure: 1.20).

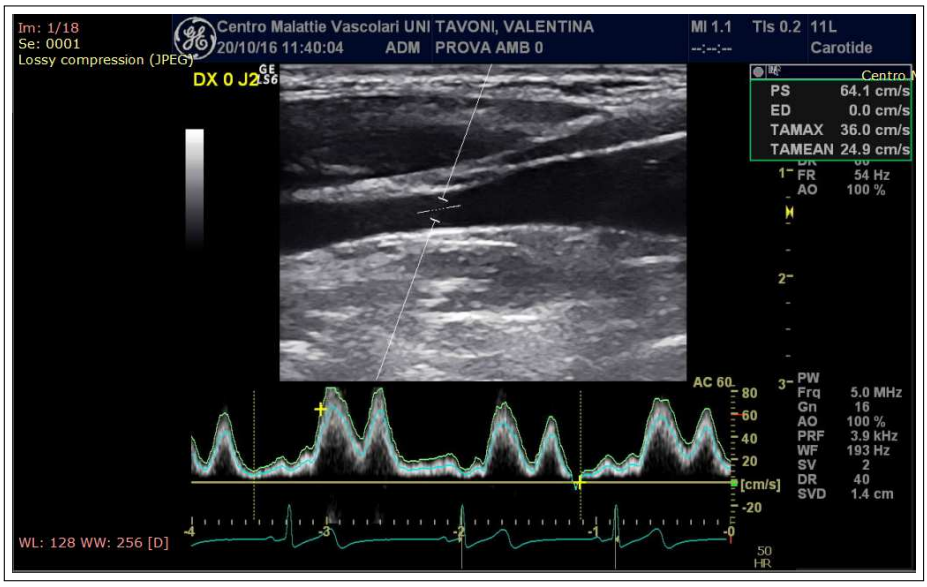

Figure 1.19: *Duplex scanning image of a blood vessel.*

The *uniformity* is the ability of the device to display an image as clean as possible. This property is quantifiable with the signal to noise ratio, and defines the smallest and the largest detectable changes in the echo amplitude. The relative brightness of the image is important because it allows to distinguish tissues from brightness random fluctuations.
The *depth of penetration* defines the major distance from where the signal arrives. On the contrary, the *dead zone* is the region close to the probe from where the signal is not able to be detected. The *beam profile* is the shape of the US beam. *Vertical* and *horizontal distance* tests determine the accuracy of measurements collected along the beam, and in perpendicular way, and visualized on the screen of the device. The *spatial resolution* determines the smallest distance between targets that can be resolved. The image of a target point generated by a real imaging system appears as a blurred dot because of the beam width and the pulse length. The *lateral resolution*, that is the minimum distance so that two objects in the image plane are distinguishable, is equal to half the beam width. The *axial resolution* determines the smallest separation between targets on the beam axis and it is equal to about half the pulse length. Thanks to the *anechoic cylinders* test, it is possible to determine the capacity of the device to identify a structure, placed at different depth, that does not produce any echo signal. The grey scale is the instrument for evaluating the dynamic range of the US device.

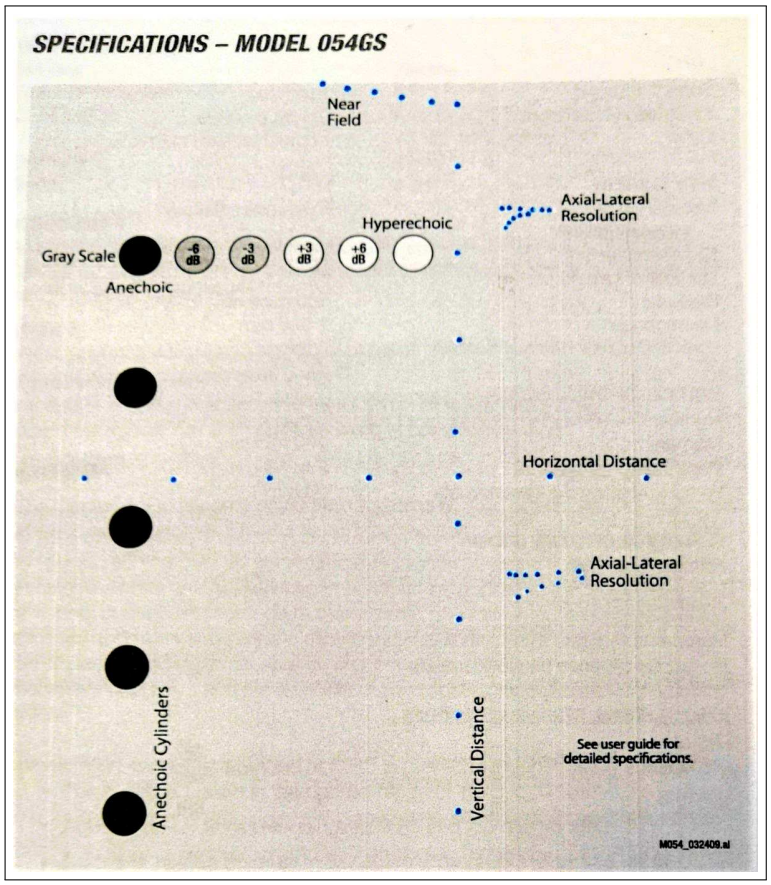

Figure 1.20: *Representation of the phantom test groups: Near Field, Grey Scale, Axial-Lateral Resolution, Horizontal and Vertical Distance, Anechoic Cylinders.*

1.4.5 Source of Errors

Different errors can occur during a US examination, all of which can lead to erroneous measurements. Some errors could be systematic: they are caused by the instrument's lack of precision or related to the methods of measurement used to assess velocity or area. An example of systematic error regards mean velocity quantification. Velocity measurements are provided by the device as values mediated over the entire SV (see equation 1.15). This implies the assumption that the intensity of the US beam is equal all over the insonated area. Unfortunately, this condition is often false and the velocity value can be subject to significant errors [55]. Moreover standard US devices require precise knowledge of the incidence angle θ in order to calculate the velocity (See equation: 1.14). It is worth noting that, with the linear probe the insonation angle never corresponds to a single value,

but rather to a range of values; this leads to an effect known as Intrinsic Spectral Broadening (ISB) [61]. The ISB implies an overestimation of the calculated velocity [62]. To overcome such problems, a calibration of the devices is necessary. This practice allows to know any device limits and to evaluate the correction factor to apply on each measurement.

Other errors could be accidental such as an incorrect settings of the system during the exam: erroneous or variable position of the patient, bad choice of the PRF and inaccurate location of the probe. The right way of measuring the CSA with the B-mode, is with the probe perpendicular to the axis of the vessel. Moreover, in order to calculate the flow, the point where the probe recorded the B-mode image and the Doppler trace should be the same. If these conditions are not respected, then some errors may occur [55]. As previously said, if the PRF is wrong, aliasing can arise. This phenomenon disturbs the signal and can cause an underestimation of the measurement. The aliasing is recognizable from the Doppler spectrum, since the signal exhibits incorrect peaks.

An error could be also determined by the inter-observer and intra-observer variabilities [63–65], since the US technology is operator dependent. In order to reduce these variabilities, several investigators attempted to measure the cerebral venous outflow by means of a quantitative US protocol. Nevertheless, such a protocol requires very skilled personnel and a long period of time to collect measurements [5, 66, 67]. In particular, the technician has to pay attention when positioning the US probe along the vessels: it is important to avoid pressing on the subject's skin, because the veins could collapse and temporary change their CSA. Moreover, the technician has to manually adjust the orientation of the US cursor, which must be parallel to the blood flow [55]. This operation allows the system to calculate the insonation angle between the US line and the blood flow. The choice of this parameter is fundamental for calculating the blood velocity (see equation 1.14). An error of only a few degrees on this angle can lead to a large underestimation, or overestimation, of the result.

1.4.6 ULA-OP

In recent years new US systems are developing, aiming to overcome some of the issues encountered with existing devices. An example of novel system is the ULA-OP developed at the University of Florence in 2009 [18]. The ULA-OP consists of a metal rack connected to a PC, where a dedicated software runs, and a probe for US examination (Figure 1.21). The rack contains 2 main boards: an analog board, which includes the

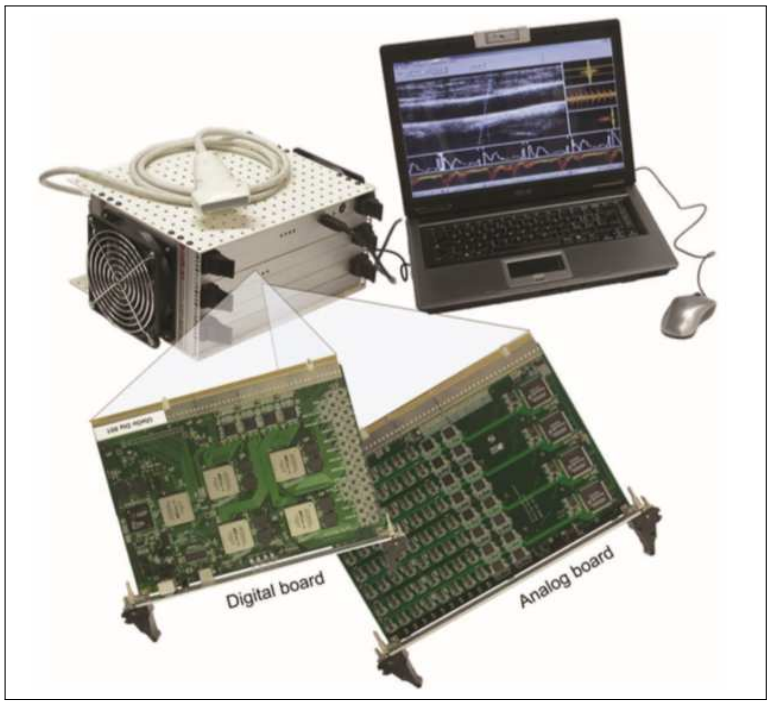

Figure 1.21: *ULA-OP system. Reproduced from [18].*

Radio-Frequency front-end, and a digital board hosting the devices in charge of numerical signal processing.

The major features of the ULA-OP system are high programmability and wide accessibility to raw data. Therefore it is suitable for a wide range of uses in several experimental research activities. The accessibility has been implemented at 4 levels: prebeamforming, Radio-Frequency postbeamforming, demodulated postbeamforming, and video data storing. In principle, it is possible to implement in the ULA-OP a lot of Transmission-Reception (TX-RX) modalities: the computational power is high enough to guarantee that a large number of processing methods work in real time.

The system flexibility and computational power of the ULA-OP are used, for example, to detect with high detail an atlas of blood velocity profiles in large human vessels. This aim is pursued through the combination of B-mode and Multigate Spectral Doppler (MSD) mode [68], which estimates the spectra of Doppler echoes produced by a M-line with 512 aligned sample volumes suitably placed over a Region Of Interest (ROI). As a result of this TX-RX strategy, the PC continuously displays morphological images of the ROI together with hemodynamic information related to the Doppler M-line [18].

Another important innovation of the ULA-OP is the vector Doppler method with an independent control of 2 US beams: reference and measuring. The first beam is used to identify the flow direction, and the second one directly estimates the true flow velocity at known beam-flow angle. Once the operator located the SV in the ROI through the extraction of certain parameters from the Doppler spectrum, reference and measuring beam are automatically turned toward the right orientation to the flow, forming a suitable Doppler angle. The velocity magnitude is thus quantified [69, 70]. Thanks to this instantaneous and automatic way to estimate the Doppler angle of insonation, it is possible to state that ULA-OP has a nominal better accuracy and precision in measuring velocity than standard devices [71].

2 *Methods*

In this thesis work two separate experimental projects, with different aims, were set up in parallel way.

First project “HC vs MCI” was intended to evaluate the presence of statistical hemodynamic differences between HC subjects, older than 50 years old, and MCI patients. The examinations have been conducted in outpatient clinic using non-invasive US technology. The evaluated hemodynamic parameters were: arterial blood inflow to the brain, blood velocity and outflow in jugular veins, JVP trace and waves of the JVP.

Second project “JVP vs CVP” aimed to verify, in an experimental way, the correlation between US JVP and CVP, invasively measured with a CVC. Each subject involved in this study was previously operated in clinical surgery by specialised staff. During the operation a physician inserted a CVC into the superior vena cava for monitoring the health condition of the patient. For each surgical subject, US examination and CVP measurement were recorded simultaneously.

The post-processing of stored data was done off-line. First of all images and video clips were elaborated with the software $Image - J$ to obtain vectors of values necessary for the analysis. Subsequently the $Matlab$ toolbox “Discrete Wavelet Transform" (DWT) and R software were used to highlight the contributions of the heartbeat to the whole signal and conform the length of the traces. At that point other useful parameters were calculated: JVP waves, mean blood flows and compliance values. One value of compliance was quantified per person: knowing for each person this value and CSA(t), we calculated a vector of pressure values. Finally the obtained traces were analysed with several methods: for the *JVP vs CVP* project we used Cross Correlation, Linear Fit and Receiver Operating

Characteristic (ROC) Curve, instead Mann Whitney U test and Principal Component Analysis (PCA) were used in *HC vs MCI* project.

US experimental sections of both the projects were executed with the same device, GE LOGIQ S6, and the same probe, GE 11L, that were previously tested with a quality control process.

At the end of the thesis work, we studied a novel US system, making a comparison with the performance of a standard device. The novel US system is an experimental platform called ULA-OP (see section *1.4.6*). During the test we compared both the modalities useful for a vascular examination, the Doppler mode and the B-mode. The test was done in-vitro for the Doppler mode and in-vivo for the B-mode. The comparison was analysed with the Student T test and Cross Correlation.

This chapter is divided as follows:

1. Quality control test on the US device, GE LOGIQ S6;
2. Methods used to collect signals with US device and CVC catheter;
3. Steps for post-processing the signals;
4. Test to compare the results;
5. Comparison between a new US device, ULA-OP, and a Traditional one.

2.1 Quality Control Test On US device

Quality control test has been performed on the US device GE LOGIQ 6 with the linear probe, GE 11L, manually positioned over a phantom. The phantom used was the CIRS, Model 054GS, Norfolk, Virginia, USA [60]. It is a parallelepiped 17.8 x 12.7 x 20.3 *cm*, with an upper window for the probe, composed of a material that simulates the acoustic properties of human soft tissue; therefore this is specific to assess imaging performance of an US system. It contains several series of targets that will appear brighter or darker than the background, they allow to complete 9 different analyses on the image properties, and one for calculating the variability on each measurement (Figure 1.20).

During every check the operator applied coupling gel to the scanning surface and positioned the transducer in a vertical plane, paying particular attention to avoiding excessive pressure to not compress the target and skew the measurements. The operator adjusted the instrument settings and aligned the probe with the target to better display the spots. Once the image was optimal, it was frozen to obtain a hard copy. In post-processing both the system software and Image-J software were used to measure distances, dimensions or grey levels. Once the results were recorded, the operator compared measured values with the nominal ones reported on the phantom manual. Where not specified, each test has been carried out at the lowest and highest frequency of the device corresponding to 8 and 12 MHz. The performed analyses were:

Repeatability Test

This analysis was carried out in post-processing by measuring a diameter on the same image for 20 times. The image, acquired at the lowest frequency of the device, was the cylinder with attenuation of 3 dB in the grey scale test. The operator variability was calculated as Coefficient Of Variation (COV) defined as:

$$COV = \frac{Standard\ Deviation}{Mean\ Value}\ . \tag{2.1}$$

Uniformity

For this test 4 ROI were placed (left and right, at top and bottom) within the area of the image free of targets. In post-processing average and standard deviation of grey level within each ROI was quantified. The ratio

between average and standard deviation is equal to signal to noise ratio of the image.

Near Field - Dead Zone

Here, the operator counted how many wires of the near field target were visible during an US examination. Then, the obtained image was compared with the one reported on the phantom manual.

Depth of Penetration

Similarly to the near field test, also for this analysis the operator counted the number of target and compared the stored image with the one of the manual to calculate the distance in cm. In this case the group of interest is the vertical distance one.

Beam Profile

To individuate the shape of the beam profile, the operator acquired an image of the vertical distance group. In post-processing each target of the group was measured and its half size was reported on a graph. The obtained results were compared with the nominal curve.

Vertical Distance

In the same image of the vertical distance group, the operator measured the distance between two consecutive spots.

Horizontal Distance

To test the distance on horizontal axis, the procedure is equal to what done before. In this case the group is the Horizontal Distance one.

Axial and Lateral Resolution

For this check axial and lateral resolution groups were used. The stored images were compared with the ones reported on the manual and the relative tables.

Anechoic Cylinders

The test consisted in measuring height and width of anechoic cylinders visualized in stored images, and comparing the result with the nominal diameter.

Grey Scale

Similarly to Anechoic Cylinders analysis, height and width of 6 cylinders were measured. In this case cylinders belonged to grey scale group, from anechoic to hyperechoic.

2.2 Collect Signals

This study was conducted in accordance with the Ethical Standards of the Committee on Human Experimentation of the Hospital of Ferrara. All the volunteers signed an informed consent form. The examinations were performed by a specialised staff composed of physicians, physicists and technicians. Every volunteer was stored with a personal Identification number (ID), together with their age and gender.

US Measurement Protocol

For doing the US examination, a measurement protocol was applied. This procedure should lead to an objective, reproducible and accurate US study of the patient, made as quickly as possible. The steps of the protocol describe the correct sequence and execution of echo-Doppler measurements. Every stage is intended to reduce to a minimum the errors in processing of morphological and hemodynamic measurements. The repeatability and accuracy of the protocol has been preliminarily evaluated by applying it to a group of healthy subjects and then comparing the outcomes to a group of patients with CCSVI and multiple sclerosis [5].

The subject was placed in supine position, avoiding flexion, hyperextension and rotation of the neck, which may compress the veins and influence the measurements. The head was in a natural position and the look was facing straight up. Three electrodes were placed on the chest of the subject for simultaneously measuring the ECG signal. Before the exam, the operator should verify the quiet breathing of the subject and its hydration. During the execution a large amount of ultrasound gel was needed, in order

to avoid excessive pressure on the patient's neck. Moreover, the use of the gel ensured a complete adhesion between transducer and skin, avoiding artefacts in the image. Every image of a subject had to be recorded with a note about the studied vessel and the position of probe and patient and, finally, stored in a study with the ID of the subject.

By convention the examination started on the right side of the patient lying in supine position and continued on the left side. The IJV was studied at first: it was examined recording a B-mode video clip for CSA measurements and detecting blood velocity with Doppler mode. Then CCA and VA were studied with Duplex scanning to measure simultaneously Time Average Velocity (TAV) and diameter of the vessel.

The entire protocol was applied to the volunteers of the outpatient project (*HC vs MCI*). Differently, during the surgery project (*JVP vs CVP*) we preferred to use a short procedure to simplify and accelerate the measurements. With the short protocol only IJVs CSA and velocity were studied.

Recording a clip for IJV CSA measurements

The examination started by placing the probe in a transverse plane with respect to the length of the vessel, at the level of the thyroid gland (J2 level), as shown in figure 2.1. Here the operator focused the IJV CSA and adjusted the parameters (contrast, brightness, etc.) to point out its edges. Then the operator stored a B-mode video-clip of 10 *sec* (Figure 1.13). This time was enough to record several cardiac cycles and two or three respiratory cycles. Together with the B-mode images, the ECG trace was automatically stored, the operator had only to verify, if the trace was visible and clear in every frame of the video-clip.

Detection of Velocity

To quantify blood velocity it was necessary to study the vessel with a longitudinal scan. It was recommended to observe flow direction at first via colour flow imaging, adjusting the PRF to avoid aliasing. Subsequently, the operator performed a spectral Doppler analysis, preferably with the Duplex scanning, positioning the SV, as big as the entire lumen, in the center of the vessel. The segment indicating the beam direction had to be parallel to the vessel, forming an insonation angle as close as possible to 60°, in order to avoid measuring errors. Once the SV was positioned in the right way,

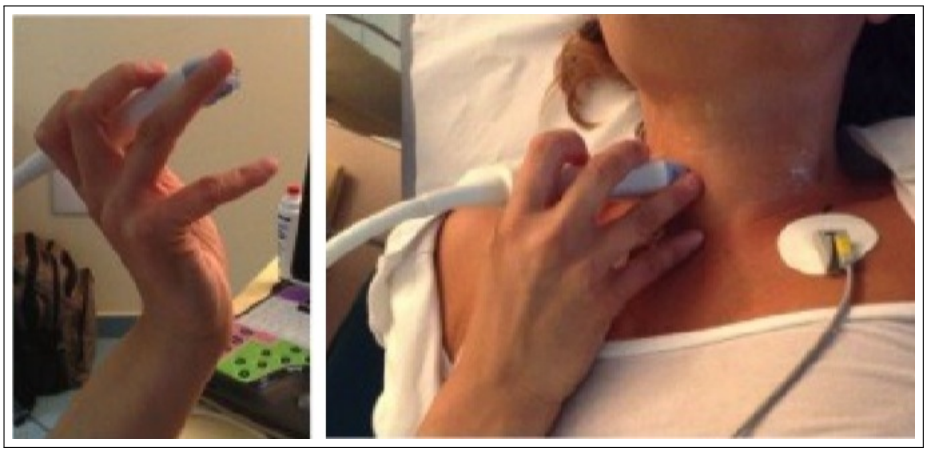

Figure 2.1: *Vascular ultrasound examination, cross sectional area measurement: correct probe handling and positioning on the neck of the patient.*

the device graphed the velocity profile and automatically calculated the TAV, i.e. the mean velocity value over the measuring time. The operator froze and stored the Duplex image with both B-mode representation of the vessel, both velocity trace (Figure 1.19). Also in this case, the ECG trace was automatically recorded together with the velocity measurements.

CVP Measurement Protocol with CVC

The subject, previously operated, was placed in supine position; his body remained static for the entire measurement time to ensure accurate and comparable results. Three electrodes were placed on the chest of the subject for simultaneously measuring the ECG signal. The CVC was attached to intravenous fluid within a pressure bag inflated up to 300 $mmHg$ [72]. The transducer, positioned to the phlebostatic axis as near to the right atrium as possible, was connected to an analogic monitor together with the ECG electrodes (Figure 1.5). To observe the CVP trace a calibration was necessary. The physician had to turn the three-way tap off to the patient and open the system to the atmosphere, press the zero button on the monitor and wait for the calibration to occur. When "zeroed" was displayed, he closed the system and turned the tap on to the patient. Once the CVP trace appeared on the monitor, it was possible to store the images on a computer by using a video capture device and its software (Figure 2.2). Every image of a subject had to be stored in a study with the ID of the patient.

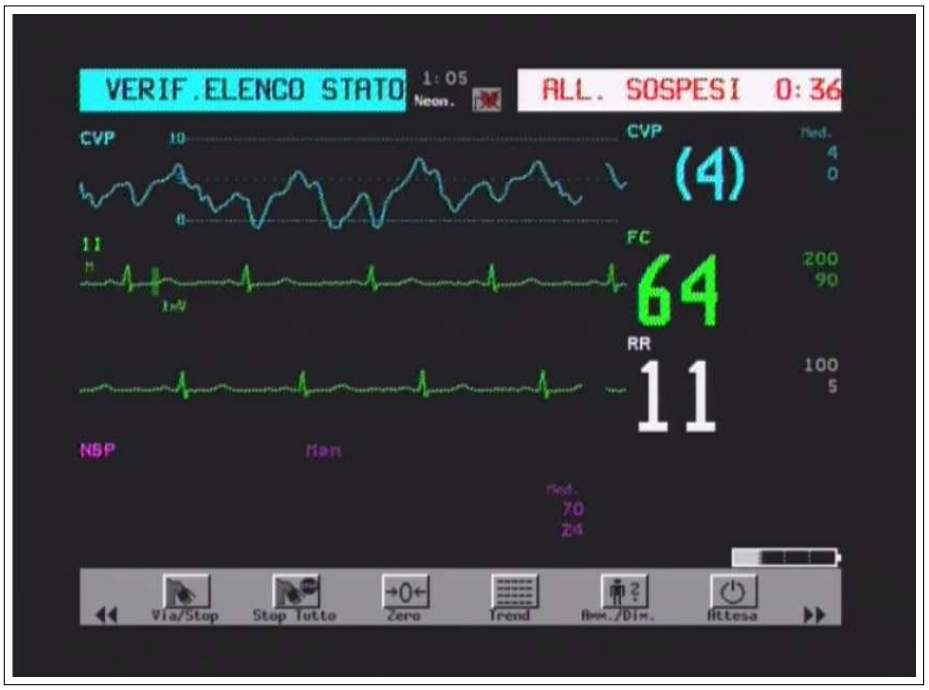

Figure 2.2: *Image of a central venous pressure (CVP) measurement, in blue the CVP trace, in green the electrocardiogram.*

2.3 Post-processing

In a second time, stored images and video clips were digitally elaborated off-line to obtain numerical data-set ready for the analyses. These were archived with the same ID as the original traces.

Analysis of CSA images

CSA data sets were produced by processing transversal video clips [6]. Each acquired sonogram sequence was opened with *ImageJ* software [73]. It allowed to measure, frame per frame, area ($pixel^2$), perimeter ($pixel$) and grey level of a selected ROI. The procedure to obtain a CSA data set consisted of several passages both manual and automatic. First of all the operator needed to know the dimension of the pixel in cm^2, time duration and number of frames of the clip, in order to calibrate the system. Then, on the first sonogram, the operator manually traced a ROI including the IJV and launches a specific customized plug-in (Figure 2.3), which automatically detected the change in shape of the given ROI throughout the video clip [6, 7]. We used two versions of the plug-in with different algorithms: one recognized regions with different grey level, the other was

able to individuate movements of IJV boundaries through time using cross correlation. The procedure provided the IJV CSA values in cm^2 versus sonogram acquisition time (Figure 2.4), that is the CSA(t) function, or Ultrasound Jugular Diagram (USJD), or JVP trace (See section *1.3*).

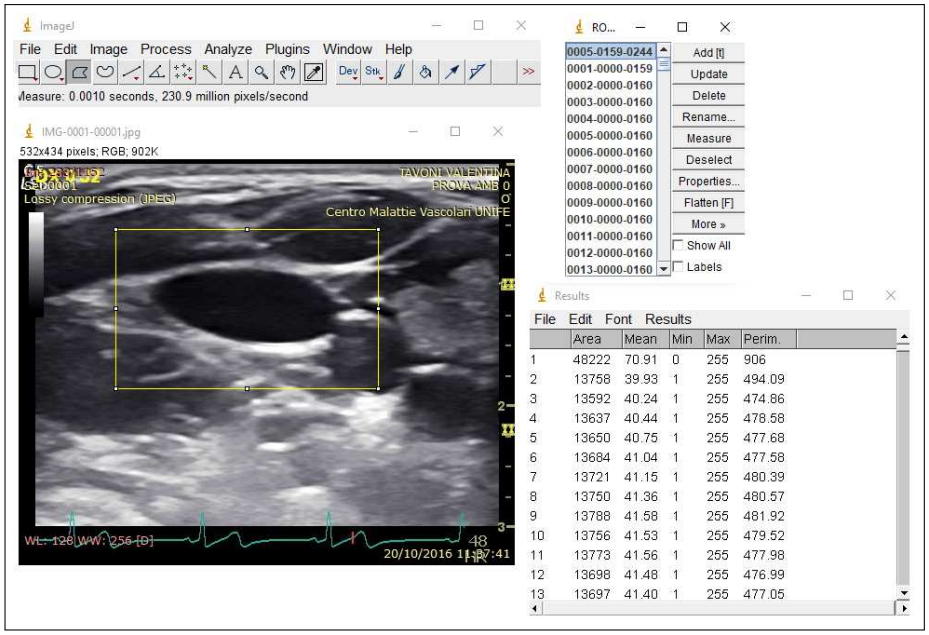

Figure 2.3: *ImageJ custom plugin to detect area variations. In figure are visible an example of B-mode image with a rectangular Region of Interest (ROI), a list of ROI and the collected measurements.*

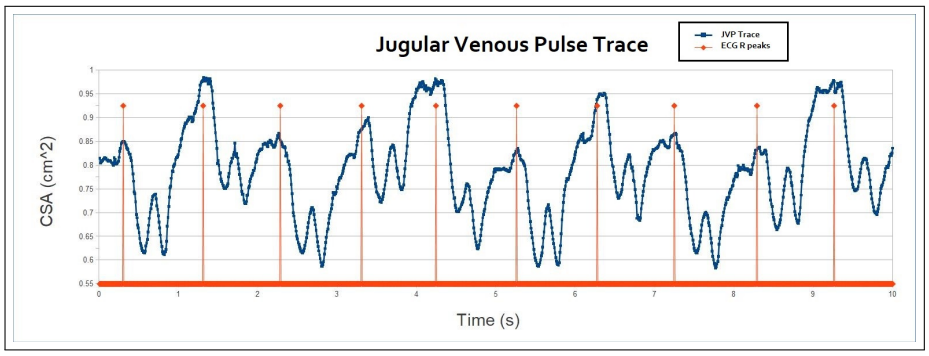

Figure 2.4: *Plot of the jugular venous pulse (JVP) trace over time obtained with the ImageJ custom plugin in blue, the R peaks of the electrocardiogram in red.*

Analysis of CVP images

The CVP data set was produced by digitally identifying the position of each point of the CVP trace on the acquired image. By using the *ImageJ* software, the operator drew a freehand line overlapping the measured trace; with the function "List Selection Coordinates" it was possible to obtain a vector of coordinates (expressed in pixels) of every point of the line. To calibrate each position, with respect to the y scale in $cmH2O$, it was necessary to rescale the measures knowing two coordinates of the y axis (Figure 2.5), as follows:

$$Y(cmH2O) = [Y(pixel) - min(pixel)] \cdot \frac{\delta(cmH2O)}{\delta(pixel)} + min(cmH2O) \quad (2.2)$$

where Y is the vertical position of one point of the trace, min is the coordinate of the inferior point on y axis, δ is the difference between the superior and inferior point on y axis. The rescaled data-set was measured in $cmH2O$.

Figure 2.5: *Calibration of the y scale: 1 and 2 are the inferior and superior points on y axis, 3 is one point Y on the trace.*

Analysis of Velocity images

The procedure for producing Velocity data sets was the same used to identify the CVP trace. The unit of measure, in this case, was the cm/s.

ECG trace

As already mentioned, an ECG trace was overlapped on each B-mode video clip, Doppler and CVP image. This trace was introduced to find a temporal scale (x axis) equal for every trace of a subject. The ECG was

represented as a movable cursor tracing the line: the position of the cursor determined the ECG value in time when each point was acquired. The ECG acquisitions and the ones of the main trace were simultaneous. The data set was created by identifying the coordinates (x,y) of every point of the trace, with the function "List Selection Coordinates" of *ImageJ*.

To set a common temporal scale, it was requested to recognize and count the R peaks in the ECG trace, starting from 0, and rescale time in Fractions of Cardiac Cycle (FCC). It was worth noting, however, that the number (N) of acquisitions between two R peaks could change, so it was important to rescale the x position of each ECG point (k) in every cardiac cycle (i):

$$FCC_{k,i} = \frac{k_i}{N_i} \tag{2.3}$$

with $i = 0$ to (number of R peaks – 1) and $k = 1$ to N .

At this point, the temporal scales (x-axis) of JVP, CVP and velocity functions were replaced with the respective vectors rescaled in FCC.

Cleaning of CVP e CSA traces

CSA(t), Velocity(t) and CVP(t) traces contain a lot of information due principally to cardiac pulsations, respiratory cycles, muscular movements and noise. The main difference between these components is their frequency. The heart rate could range between 50 to 120 beats per minute, therefore the frequencies widely above 2 Hz or below 0.8 Hz, could be noise or breathing contribution respectively. There are different techniques for analysing a signal and removing non-cardiac trends from measured data: some produce results localized only in frequencies, some others give results in both time and frequencies. This last type of methods, as the DWT, is the only one that allows to reconstruct the analysed signal [74]. Since DWT technique was already used in two different works to analyse JVP traces [75, 76], and previous studies demonstrated that Fourier- and Wavelet-based analysis yield equivalent results [77–79], in the present work we used the DWT approach, that is already implemented in a *Matlab* Toolbox. In this type of analysis, the signal is convolved for a certain number of times with a filter, called wavelet. Using the function "Wavelet 1-D", it is possible to choose the shape of the wave and decide how many times reiterate the division of the signal. After each step, the software shows the signal without the contribution of one range of frequencies (Approximation, a_i) and the contribution itself (Detail, d_i). The most prominent components in the

original signal appear as high amplitudes, on the contrary, the frequency bands less prominent have very low amplitudes, and their contributions can be discarded from the raw signal without any major loss of information. The wavelet family that most describes the details of JVP cycles is the Symlet one. In this work, we opted for Symlet 7, choosing maximum level of reiteration.

An example of recorded trace with its DWT filtered curves is reported in figure (Figure 2.6).

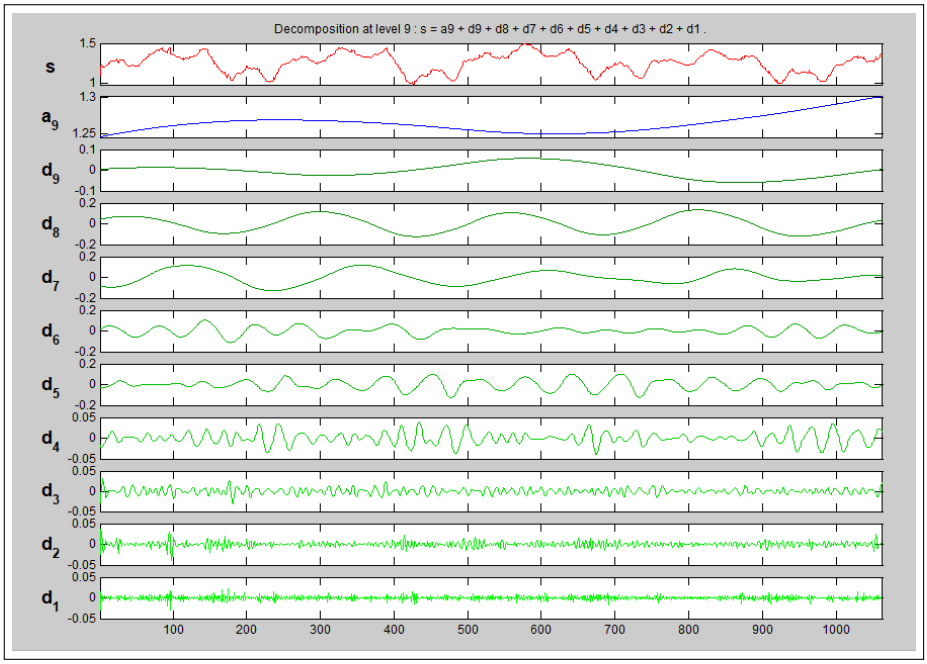

Figure 2.6: *Wavelet analysis of the signal with Matlab toolbox. s is the original signal, d1, d2 and d3 the details at higher frequencies than cardiac cycle, d4, d5 and d6 the details at frequencies close to cardiac cycle, d7, d8 and d9 the details at lower frequencies than cardiac cycle, a9 the signal without the details.*

The lowest curves ($d1$, $d2$, $d3$) show the highest frequencies of the signal (widely above 2 Hz), in the center are visible mean frequencies details ($d4$, $d5$, $d6$) and the lowest frequencies (widely below 0.8 Hz) contributions ($d7$, $d8$, $d9$). At the top there is the entire raw signal (s) and, just below, the signal without all the already mentioned components ($a9$). Knowing that video clip has on average a frame rate around 80-100 fps, the highest frequency components have a rate of several tens of Hertz, the lowest frequency components have a rate of few tenths of Hz, while mean details

have a main frequency around a few Hz.

To reconstruct the signal highlighting the contribution due to the heartbeat, we summed the mean frequencies details to the mean value of the raw signal:

$$CSA(t) = MeanValue + d4(t) + d5(t) + d6(t). \tag{2.4}$$

Using the resulted function, we built a vector of values for each trace.

Conformation of the traces

Finally, the last step of the off-line elaboration was the conformation of the traces of same subject: each trace was divided in its cardiac cycles (i) and they were extended to the same number of frames ($\tilde{N} = max\, N_i$).

For doing this we implemented a custom script with R software. The script was able to read a vector of values, draw the corresponding graph and perform a linear interpolation. Then, fixing the extreme points, it divided the curve in a certain number of values and created a new vector for every cardiac cycle of each trace. The entire trace was reconstructed putting together every single vector. At the end of elaboration, the number of values per each trace was

$$M = (numb.\, of\, Rpeaks - 1) \cdot \tilde{N}\ . \tag{2.5}$$

2.4 Calculation of Parameters

Once finished the post-processing elaboration on images and traces, we calculated other useful parameters for the analysis.

Mean Time Delay Analysis

JVP(t) and CVP(t) functions were synchronized using ECG, and plotted in an amplitude vs time graph. Subsequently, the traces were analysed studying amplitude and time-position in FCC of every a,c,x,v,y wave (described in section 1.3). The time-position was useful to determine the Mean Time Delay (MTD) between the two functions of the same subject. For evaluating this delay, we studied a minimum of 4 cycles per trace: for every details j we calculated the mean difference, in FCC, between the

position on x-axis of the wave and R peak of ECG. For example, the delay of j-wave was calculated as follows:

$$Delay\,JVP_j = Mean[JVP_{j,i} - R_i] \tag{2.6}$$

$$Delay\,CVP_j = Mean[CVP_{j,i} - R_i] \tag{2.7}$$

with i=1 *to* (*number of cycles*), j=a,c,x,v,y. Then we subtracted arithmetically the CVP delay to the JVP one:

$$Time\,Delay_{j-wave} = Delay\,JVP_j - Delay\,CVP_j. \tag{2.8}$$

Finally, averaging time delays of every detail, the mean time delay was obtained:

$$MTD = Mean[Time\,Delay_{j-wave}] \tag{2.9}$$

with j=a,c,x,v,y

Calculation of mean FLOW

For the *HC vs MCI* study we needed to calculate the mean blood flow, both arterial (inflow) and venous (outflow). To estimate the blood flow Q , we used this formula:

$$Q = TAV \cdot mean[CSA(t)]. \tag{2.10}$$

For calculating mean CSA in arterial vessels we used diameter values measured on B-mode longitudinal images [58].

$$Mean\,CSA_{Artery} = \pi \cdot (\frac{diameter}{2})^2 \tag{2.11}$$

Model to calculate a predicted pressure

An important parameter for *JVP vs CVP* project was the compliance value (See section *1.3*). A mean 2D compliance value was calculated for each patient, following a model described in literature [9–11]. Starting from Moens-Korteweg equation 1.2 it was possible to calculate a 2D compliance value (C') as:

$$C' = \frac{CSA_x}{\rho \cdot w^2} \tag{2.12}$$

where CSA_x is the CSA corresponding to the x wave, ρ the blood density and w the velocity of propagation of pressure wave. This velocity, defined in equation 1.2, could be experimentally calculated as:

$$w = \frac{l_G}{MTD} \tag{2.13}$$

where MTD, defined in equation 2.9, is the delay between JVP and CVP trace, while l_G is the distance between the two points of measure of JVP and CVP.

Once obtained the compliance value for each patient, knowing CSA(t), we calculated pressure variations following equation 1.8.

Difference between CVP and predicted pressure

CVP and calculated pressure are quantified in different place of the circulatory system: vena cava and IJV. The distance between the points where the measures are taken, could lead to a difference in pressure. This quantity can be calculated using the Poiseuille's Law:

$$\Delta P = \frac{8\mu l_G}{\pi r^4} \cdot Q \tag{2.14}$$

where Q is the blood flow within the IJV, μ is the blood viscosity, l_G is the distance between the points of measure, and r is the radius of the vessel (supposed to be circular).

2.5 Statistical Analysis

Once obtained all the parameters useful for the studies, we implemented the analysis.

2.5.1 HC vs MCI Project

Mann Whitney U Test

With this analysis, our aim was to determine statistical differences between any of the parameters of the two populations. Since the samples had non-gaussian distributions and were independent, we used the non-parametric Mann-Whitney U test [80]. This test is able to verify whether the samples were selected from the same population or from populations having the

same distribution. The null hypothesis is rejected if p-value is lower than 0.05.

Principal Component Anlysis

We built a graph of the obtained results using the principal component analysis [81]. Our aim was to find some trends in the distribution considering Age of the subject, IJV CSA and blood Velocity.

2.5.2 JVP vs CVP Project

Cross Correlation

We started the analysis evaluating, for each subject, the level of similarity between JVP(t) and CVP(t) as a function of a temporal shift of one relative to the other: the technique used is called Cross Correlation [82]. This approach is useful to determine also the time delay (LAG) between the traces: the maximum of Cross Correlation function indicates the instant when the signals are best aligned.

For applying Cross Correlation we created a custom script in *R*. The software read the vectors, applied the illustrated technique and returned the maximum value of correlation and the LAG (in frames).

Knowing the total number $\tilde{N}$ of frames in a cardiac cycle, we were able to determine the LAG in Fraction of Cardiac Cycle (FCC).

$$LAG(FCC) = \frac{LAG(number\,of\,frame)}{\tilde{N}} \tag{2.15}$$

Linear Fit

To evaluate whether the Compliance model is able to predict pressure values close to CVP measurements, we built a graph of CVP against Calculated Pressure. On the graph a linear fit was applied together with the ideal profile: the correlations parameters were reported in a table.

Receiver Operating Characteristic Curve

To evaluate sensitivity and specificity of our model, we used the Receiver Operating Characteristic (ROC) curve [83]. This technique allowed to estimate the maximum capability of a model in predicting true results, changing time by time the threshold of classification.

2.6 ULA-OP

In this last section we studied the performances of the ULA-OP, a novel US device developed at the University of Florence in 2009 (see section 1.4.6). The test consisted of a comparison between ULA-OP and a standard US equipment. Firstly we tested the innovative Doppler mode implemented in the new platform and then the B-mode. The measurements done with these two modalities are an integral part of the US measurement protocol described in the above section (see section 2.2). Our aim was to understand if this device could be used, in the future, for clinical diagnostics. Doppler mode was tested in-vitro, with a phantom and a known flow inside. The measurements were collected in the Ecofluidodynamic laboratory of the department of Physics and Earth Sciences of the University of Ferrara. B-mode comparison was done in-vivo, analysing 8 volunteers. These measurements were collected by a skilled sonographer, at the Department of Biomedical Engineering of the University of Lund (Sweden).

2.6.1 Doppler Comparison

Doppler comparison was performed between two devices: a conventional US device (Technos MP, Esaote S.P.A., Genoa, Italy) and the ULA-OP platform. The US probe used during the measurements was a linear array probe (LA523, Esaote S.P.A., Florence, Italy). This was fastened to a manual positioner, which allows to move the probe in very small steps and fixing it in the desired position.

The test was performed through an in-vitro study. The circuit used was composed by a custom neck phantom and a gear pump (Figure 2.7); the liquid was a Blood Mimicking Fluid (BMF)(CIRS, Model 046, Norfolk, Virginia, USA) with the same acoustic properties of the blood. The phantom was a PMMA box (20.0 x 12.0 x 20.5 cm) full of water, containing a plastic tube with a circular CSA equal to (0.5 $\pm$ 0.1) cm^2. The tube was fixed to a goniometer indicating the insonation angle between probe and flow. The pump generated a static volume flow and drove it around the circuit simulating venous blood flow. The BMF was contained in a tank that was inserted in the circuit with a turbine flowmeter also. The flowmeter, powered by a 9 V battery and connected to an oscilloscope, was used to calibrate the pump. During each test the flow set in the pump was varied between (150 $\pm$ 1) mL/min and (650 $\pm$ 1) mL/min in steps of (100 $\pm$ 1) mL/min.

The analyses were useful to quantify repeatability and reproducibility

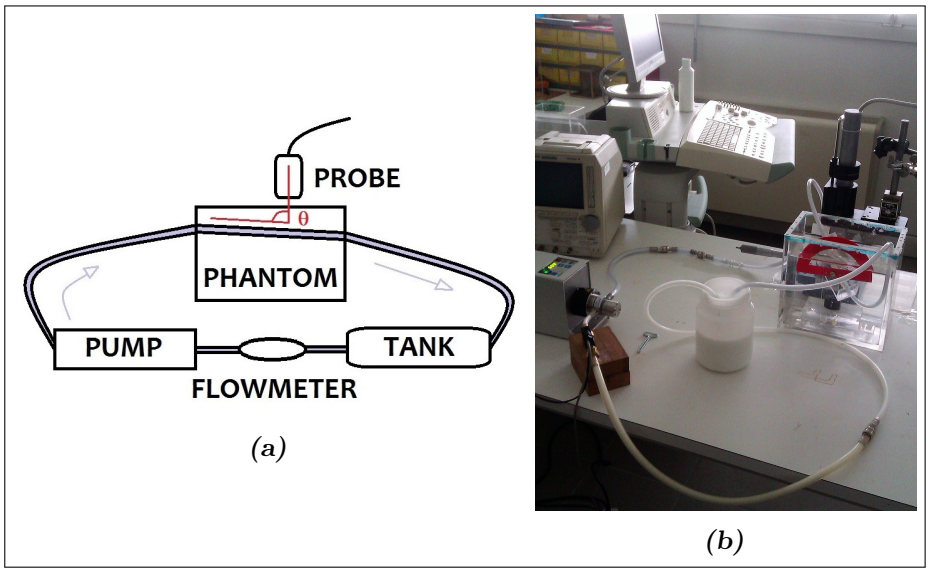

Figure 2.7: *Representation (a) and image (b) of the circuit used for the Doppler test.*

of Doppler measurements. The repeatability was tested by reiterating the same measurements during the same experimental session, for five times with the Standard device and for twenty times with the ULA-OP. The reproducibility, instead, was measured by repeating the entire procedure in different experimental sessions in order to have sufficient statistics, for five times with the Standard device and for twenty times with the ULA-OP.

Calibration test

First of all, we calibrated the system comparing flow values set in the pump with values measured by the flowmeter. The flowmeter gives a pulsed electric signal for each cycle, whose frequency was measured with an oscilloscope. The Fast Fourier transform mode of the oscilloscope provided the main frequency f, correlated to the measured flow $\phi_{flowmeter}$ with the constant $k = 22{,}000\ pulse/L$, as follows:

$$\phi_{flowmeter} = \frac{f}{k} \ . \tag{2.16}$$

With a paired t-test, we verified whether flow values measured with the flowmeter and those set in the pump were significantly different.
Following the equation 2.10, flow values were converted into velocity values through the CSA of the tube.

Test with standard device

The measurements were performed by positioning the probe over the circuit. The insonation angles used for the test of the standard device were 30°, 45° and 60° ± 1°, we chose these values following the guidelines to obtain reliable measurements. We studied the phantom using two different sizes of SV: the smallest one, equal to 1 mm, and the largest one, equal to 8 mm. Since the flow is assumed to be laminar, both the mean TAV and half of the peak TAV were stored. For every different experimental setup (angle-SV-TAV), we collected a set of measurements composed by five velocity quantifications per each flow values set in the pump.

Test with ULA-OP

The test was done using the B-MSD-SpTR-Mode of the ULA-OP. With this mode the device automatically adjusts the angle of insonation using a double US line (See section *1.4.6*) and measures the velocity in the focus point within the vessel. The experiment was performed fixing the angle between tube and probe to 80° ± 1°. The choice of this angle is given by the best setting suggested by the manufacturer to obtain reliable measurements (personal communication). The system automatically displays only the measurement of the peak velocity. With the ULA-OP, a set of measurements, composed by twenty velocity quantifications for each flow values set in the pump, was collected.

Analysis of results

Once obtained all the measurements, we calculated for each set mean value, Standard Deviation (SD) and COV. Subsequently, putting in one graph all the mean values, obtained with the same experimental setup, we calculated a linear fit of the values. Finally, paired t-test was used to state the null hypothesis that two samples of velocity measurements were not significantly different from each other.

2.6.2 B-mode Comparison

B-mode comparison was performed between two devices: a conventional US device (Epiq 7G Philips, Bothell, WA, USA) and the ULA-OP platform. The US probe used during the measurements was a linear array probe (L18-5, Philips).
The test was performed through an in-vivo study with 8 healthy volunteers.

As described in section 2.2, the subject was placed in supine position, with the head in a natural position. Three electrodes, connected to the standard device, were placed on the chest of the subject for measuring the ECG signal. The examination was performed recording a B-mode video clip of the right IJV of the subject, firstly with standard device, then with ULA-OP. The examination started by placing the probe, with a large amount of ultrasound gel, in a transverse plane with respect to the length of the vessel, at the J2 level. The operator focused the IJV CSA, adjusted the parameters to point out its edges and stored a B-mode video-clip of 10 sec. This time is enough to record several cardiac and two or three respiratory cycles. Every video-clip was stored with the ID of the subject and a note about the US device used.

Test with standard device

Together with the B-mode video-clip, the ECG trace was automatically stored, the operator had only to verify, if the trace was visible and clear in every frame of the video-clip.

Test with ULA-OP

The test was done using the B-mode modified in order to record 96 lines on x-axis instead of 192 as usual. Reducing the dimension of the images, it was possible to record video-clip with an higher frame rate about 80 fps, equal to the frame rate of standard devices. The video-clips were stored in raw format: i.e. in 3 data sheets with all the information about the stored video.

Post-processing

To process ULA-OP measurements we implemented a custom script in Matlab. The script was able to read the raw dataset and return a video-clip similar to the ones obtained with the standard device. The only differences between the video-clips are the ECG trace, not acquirable with the ULA-OP used, and the dimension of pixels. With the standard device it is possible to measure the dimension of pixels directly from the image, since in every acquisition it is visible a millimetre scale. Unfortunately in saving and reconstructing the ULA-OP measured we lost the millimetre scale, and it was impossible to convert the data from pixel to cm^2.

The obtained video-clips were elaborated as described in section 2.3: firstly they were processed with the custom script in *ImageJ* to obtain

JVP traces. Then they were cleaned with the Wavelet toolbox in *Matlab* and uniformed with the *R* software. In this case, the division of the trace was done using only the a peak of the JVP.

Analysis of results

Once obtained the measurements, the traces were compared in pairs with the Cross Correlation script, to quantify the level of similarity between the traces collected by the devices. To be thorough, we added to the script also the calculation of Pearson correlation coefficient, as a measure of the linear correlation between the variables.

Finally we tested the image quality of the ULA-OP images, measuring the Signal difference to Noise Ratio (SdNR) as described in equation (2.17).

$$SdNR = \frac{Mean\,Grey\,Levels_{\,Details} - Mean\,Grey\,Levels_{\,Background}}{SD\,Grey\,Levels_{\,Background}}. \tag{2.17}$$

3 Results

The obtained results are shown in this chapter: Quality Control Test of US device, *HC vs MCI* Project, *JVP vs CVP* Project and ULA-OP Characterisation for the Doppler mode and B-mode.

3.1 Quality Control Test

The error associated to the measumerents, in this thesis work, is the same reported by the manual of the US device in section "System data", table "Basic Measurements and Precision" [84] (GE LOGIQ S6).

Precision of Measurements	
Measurement	**Value**
Distance	5% (1-2 mm)
Area	5% (1 mm^2)
Velocity	10% (1 cm/s)
Time	5% (10 ms)

Table 3.1: *Precision of Measurements. Table reported by the manual of the GE ultrasound device [84].*

Repeatability Test

The precision of the operator, calculated as COV, was about 5%.

Uniformity

In table 3.2 are reported the mean results of signal to noise ratio.

Uniformity		
Frequency	**Close Depth**	**Far Depth**
Maximum	8	11
Minimum	6	4

Table 3.2: *Results of the Uniformity Test executed with the GE ultrasound device.*

Near Field - Dead Zone

We were able to visualize all the 6 spots of the near field group: the dead zone is less then 1 mm.

Depth of Penetration

In table 3.3 are reported the maximum depth of penetration displayed by the US device.

Depth of Penetration	
Frequency	**Maximum Depth**
	cm
Maximum	5.8
Minimum	8.8

Table 3.3: *Results of the Depth of Penetration Test with the GE ultrasound device.*

Beam Profile

The obtained curves are shown in graph 3.1: in blue the minimum frequency, in red the maximum frequency and the nominal curve is represented with the spotted grey line.

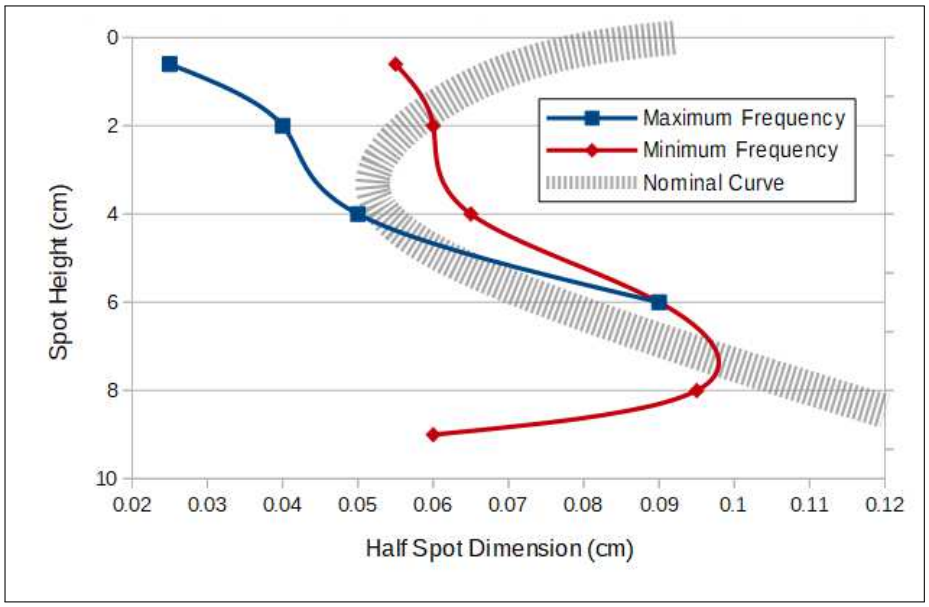

Figure 3.1: *Plot of right part of the beam profile measured with GE ultrasound device, in blue the profile recorded at the minimum frequency and in red the one at the maximum frequency, and representation of the nominal beam profile as reported by the manual with the spotted grey curve.*

Vertical Distance

In table 3.4 are reported the mean value of vertical distances between the spots of the vertical distance group. The nominal distance is 2.00 *cm*.

Vertical Distance	
Frequency	**Mean Value**
	cm
Maximum	2.0
Minimum	2.0

Table 3.4: *Results of the Vertical Distance Test executed with the GE ultrasound device.*

Horizontal Distance

The mean value of horizontal distances between the spots of the horizontal distance group is 2.0 *cm*. The nominal distance is 2.00 *cm*.

The analysis was done only for the minimum frequency, because the spots were visible exclusively with this setting.

Axial and Lateral Resolution

Comparing the stored images with the one reported on the manual, we found that axial and lateral resolution are 0.25 mm (Figure 3.2).

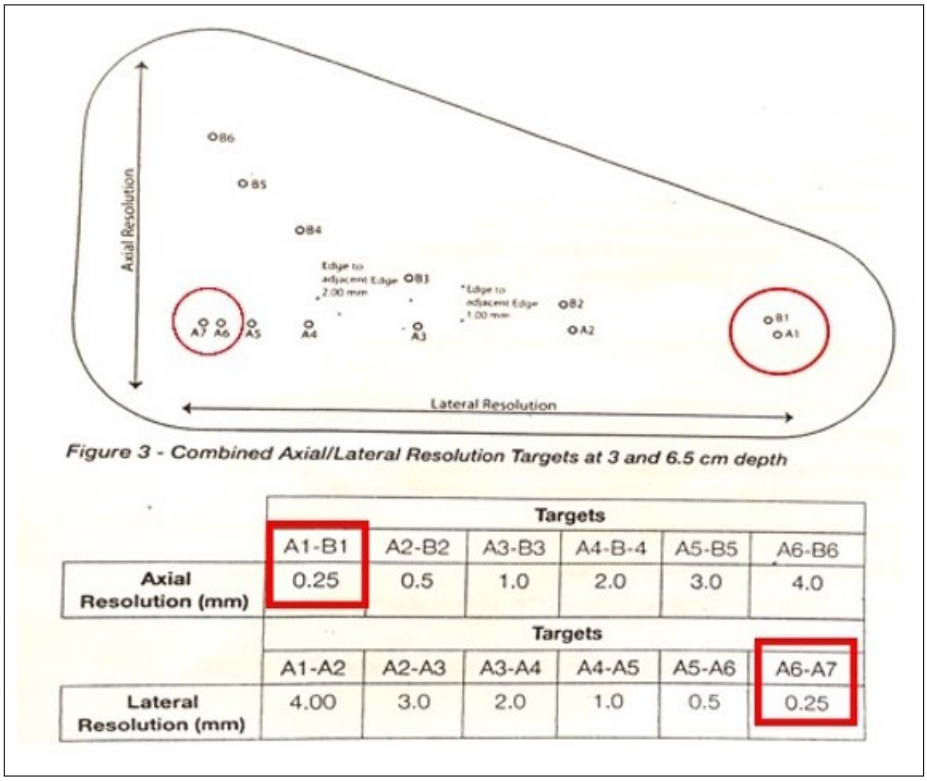

Figure 3 - Combined Axial/Lateral Resolution Targets at 3 and 6.5 cm depth

	Targets					
	A1-B1	A2-B2	A3-B3	A4-B-4	A5-B5	A6-B6
Axial Resolution (mm)	0.25	0.5	1.0	2.0	3.0	4.0

	Targets					
	A1-A2	A2-A3	A3-A4	A4-A5	A5-A6	A6-A7
Lateral Resolution (mm)	4.00	3.0	2.0	1.0	0.5	0.25

Figure 3.2: *Table of Axial and Lateral Resolution test reproduced from the manual of the phantom [60]. The results obtained with the GE ultrasound device are highlighted in red.*

Anechoic Cylinders

In table 3.5 are reported mean values of height and width measurements of Anechoic Cylinders. With the maximum frequency, only the first cylinder of the anechoic group was visible. The nominal diameter is 0.80 *cm*.

Anechoic Cylinders			
Frequency	**Cylinder**	**Mean Height**	**Mean Width**
		cm	**cm**
Maximum	1	0.7	0.8
Minimum	1-2	0.7	0.7

Table 3.5: *Results of the Anechoic Cylinders test with the GE ultrasound device.*

Grey Scale

In table 3.6 are reported the mean values of height and width measurements of Grey Scale cylinders. The nominal diameter is 0.80 *cm*.

Grey Scale			
Frequency	**Cylinder**	**Mean Height**	**Mean Width**
		cm	**cm**
Maximum	1-6	0.7	0.7
Minimum	1-6	0.7	0.7

Table 3.6: *Results of the Grey Scale Cylinders test with the GE ultrasound device.*

3.2 HC vs MCI Project

For the *HC vs MCI* Project we analysed 80 healthy subjects and 18 MCI patients. Since 6 subjects of the HC group suffered of cardiac diseases, only 74 subjects were inserted in this study. HC group was formed by 43 males and 31 females, between 50 and 72 years of age. MCI group was formed by 15 males and 3 females, between 66 and 81 years of age.

In tables 3.7 and 3.8, stored and analysed data of the HC and MCI group, respectively, are reported. Useful information for the analyses are the arterial inflow, blood velocity and flow in right IJV, Mean IJV CSA (or Mean JVP) and mean amplitude of wave a, c, x, v, y of the JVP trace. The subjects with an age between 66 and 72 are highlighted in bold.

HC Subjects Dataset

Data		Arteries	IJV			JVP Waves				
ID	Age	InFlow	Q	CSA	TAV	a	c	x	v	y
		cm^3/s	cm^3/s	cm^2	cm/s	cm^2				
1	58	18	13	0.33	39	0.50	0.43	0.27	0.35	0.24
2	57	11	9	0.84	11	0.91	0.87	0.70	0.72	0.71
3	51	14	27	0.40	68	0.44	0.39	0.34	0.39	0.36
4	59	17	12	0.53	22	0.61	0.47	0.44	0.48	0.46
5	55	15	5	0.34	14	0.42	0.37	0.30	0.32	0.31
6	61	21	2	0.16	12	0.25	0.19	0.09	0.13	0.14
7	52	19	7	0.17	39	0.17	0.16	0.15	0.16	0.16
8	59	16	20	0.44	46	0.51	0.44	0.39	0.41	0.38
9	59	13	14	0.40	36	0.63	0.49	0.29	0.44	0.34
10	50	12	13	0.61	21	0.71	0.64	0.48	0.51	0.51
11	60	16	5	0.32	13	0.43	0.36	0.24	0.33	0.33
12	60	16	3	0.19	18	0.21	0.20	0.19	0.20	0.18
13	60	9	60	1.40	43	1.57	1.40	1.23	1.39	1.35
14	59	15	12	0.41	30	0.48	0.41	0.32	0.41	0.40
15	59	9	12	1.06	12	1.21	1.12	0.95	1.03	1.01
16	56	8	12	1.04	11	1.29	1.15	0.89	0.94	0.88
17	55	12	11	1.00	11	1.20	1.08	0.89	0.98	0.92
18	58	16	12	0.37	32	0.45	0.41	0.32	0.40	0.38
19	51	-	10	0.98	10	1.08	1.07	0.94	0.96	0.91
20	51	10	6	0.22	29	0.25	0.22	0.19	0.22	0.20
21	51	4	13	0.42	30	0.51	0.44	0.31	0.40	0.37
22	58	15	3	0.18	19	0.29	0.22	0.13	0.21	0.16
23	54	-	15	2.24	7	2.52	2.45	2.24	2.30	2.26
25	56	14	19	0.66	29	0.77	0.72	0.59	0.68	0.58
27	50	14	13	0.55	24	0.67	0.62	0.45	0.48	0.46
28	61	13	23	0.57	41	0.63	0.60	0.52	0.54	0.52
29	54	14	20	0.38	53	0.45	0.42	0.32	0.39	0.37
30	64	14	13	0.99	13	1.09	1.02	0.96	1.01	0.97
31	55	-	9	0.38	25	0.46	0.37	0.30	0.40	0.40
32	50	13	28	1.07	27	1.16	1.13	1.03	1.08	1.07
33	51	13	6	1.32	4	1.41	1.38	1.29	1.32	1.28
34	54	7	8	0.80	9	0.88	0.82	0.76	0.82	0.77

HC Subjects Dataset										
Data		**Arteries**	**IJV**			**JVP Waves**				
ID	**Age**	**InFlow** cm^3/s	**Q** cm^3/s	**CSA** cm^2	**TAV** cm/s	**a**	**c**	**x** cm^2	**v**	**y**
35	59	17	10	0.21	46	0.32	0.19	0.08	0.26	0.26
37	50	13	17	0.94	18	1.15	1.01	0.79	0.84	0.84
38	58	10	4	0.22	17	0.27	0.25	0.22	0.23	0.19
39	58	11	35	0.85	41	0.97	0.88	0.80	0.88	0.84
40	54	18	12	0.24	51	0.18	0.15	0.13	0.13	0.12
41	55	12	8	0.43	18	0.53	0.48	0.38	0.41	0.37
42	52	13	9	0.44	21	0.49	0.48	0.40	0.41	0.40
43	52	11	4	0.43	9	0.48	0.45	0.41	0.45	0.40
44	52	15	15	2.09	7	2.15	2.09	2.01	2.06	2.05
45	52	14	10	1.42	7	1.51	1.47	1.36	1.42	1.40
46	52	18	12	2.11	6	2.25	2.14	2.03	2.03	1.99
47	56	-	4	0.74	5	0.84	0.79	0.57	0.74	0.66
48	55	19	16	0.88	19	0.96	0.92	0.80	0.88	0.84
49	59	12	19	0.37	53	0.44	0.38	0.31	0.34	0.31
50	52	14	10	1.09	9	1.16	1.11	1.05	1.10	1.05
51	52	15	11	0.43	25	0.61	0.52	0.31	0.42	0.40
52	51	18	5	0.18	27	0.22	0.19	0.16	0.17	0.14
53	55	14	5	0.48	10	0.50	0.50	0.46	0.46	0.44
55	56	12	18	1.12	16	1.45	1.35	1.20	1.25	1.18
56	51	15	16	2.04	8	2.20	2.16	2.05	2.06	2.05
58	55	13	7	0.19	39	0.22	0.20	0.18	0.19	0.14
59	52	18	3	0.32	9	0.33	0.32	0.32	0.33	0.32
60	58	13	36	0.90	40	0.99	0.94	0.86	0.95	0.81
61	59	21	24	0.41	58	0.47	0.42	0.38	0.40	0.36
62	64	19	19	1.51	12	1.63	1.57	1.47	1.44	1.40
63	55	15	28	0.80	35	1.00	0.97	0.72	0.79	0.72
64	**67**	13	17	2.45	7	2.62	2.47	2.31	2.48	2.49
65	**67**	18	8	0.31	27	0.40	0.31	0.26	0.34	0.28
66	**68**	19	46	2.66	17	2.73	2.71	2.68	2.71	2.67
67	**69**	11	12	1.25	10	1.27	1.24	1.22	1.28	1.24
68	**68**	13	5	0.47	11	0.50	0.47	0.44	0.46	0.43
69	**69**	17	23	1.39	16	1.49	1.38	1.27	1.39	1.39
70	61	21	17	0.87	20	0.95	0.93	0.80	0.84	0.83
71	53	7	6	0.52	12	0.61	0.60	0.47	0.52	0.47
72	**68**	-	7	0.61	12	0.81	0.75	0.50	0.58	0.51
73	**66**	-	4	0.56	8	0.71	0.64	0.45	0.55	0.05
74	**72**	17	22	1.24	18	1.28	1.28	1.21	1.27	1.21
75	**70**	-	11	0.63	17	0.72	0.64	0.57	0.64	0.59
76	59	13	46	1.77	26	1.91	1.73	1.65	1.76	1.71
77	**66**	11	5	0.32	15	0.50	0.29	0.17	0.38	0.30
78	51	11	19	0.56	33	0.65	0.59	0.50	0.52	0.48
79	65	17	7	2.11	3	2.13	2.12	2.10	2.11	2.10

Table 3.7: *Dataset of healthy control (HC) subjects: ID, age, arterial (Inflow) and venous flow (Q), internal jugular vein (IJV) area (CSA) and velocity (TAV), waves of jugular venous pulse (JVP). Subjects in bold are in the interval age between 66 and 72 years.*

MCI Patients Dataset										
Data		**Arteries**	**IJV**			**JVP Waves**				
ID	**Age**	**InFlow** $\mathbf{cm^3/s}$	**Q** $\mathbf{cm^3/s}$	**CSA** $\mathbf{cm^2}$	**TAV** $\mathbf{cm/s}$	**a**	**c**	**x** $\mathbf{cm^2}$	**v**	**y**
1	**66**	-	7	0.26	28	0.31	0.29	0.26	0.28	0.27
2	**68**	-	16	1.76	9	1.93	1.73	1.60	1.73	1.67
3	**69**	-	4	1.61	2	1.94	1.85	1.34	1.45	1.41
4	73	-	11	2.01	5	2.11	2.06	1.94	2.02	2.01
5	74	11	29	0.88	33	1.00	0.90	0.84	0.90	0.86
6	**68**	14	0	0.66	1	0.62	0.58	0.41	0.42	0.41
7	75	14	3	0.29	12	0.33	0.29	0.25	0.29	0.28
8	**72**	20	11	0.57	20	0.62	0.56	0.52	0.56	0.52
9	81	21	20	1.03	19	1.05	1.02	0.95	1.02	0.96
10	**67**	12	6	1.76	3	1.97	1.88	1.72	1.81	1.77
11	78	16	13	1.08	12	1.23	1.10	1.06	1.11	1.08
12	79	-	2	1.89	1	2.51	2.11	1.24	2.07	2.11
13	75	-	1	0.11	13	0.14	0.11	0.10	0.11	0.09
14	**68**	18	25	2.31	11	2.58	2.32	2.19	2.27	2.22
15	**68**	14	26	2.05	13	2.19	2.10	1.99	2.02	2.01
16	**67**	-	24	0.58	41	0.67	0.61	0.54	0.57	0.55
17	79	24	15	1.30	12	1.42	1.36	1.23	1.27	1.26
18	81	9	12	1.28	10	1.36	1.32	1.25	1.30	1.25

Table 3.8: *Dataset of mild cognitive impairment (MCI) patients: ID, age, arterial (Inflow) and venous flow (Q), internal jugular vein (IJV) area (CSA) and velocity (TAV), waves of jugular venous pulse (JVP). Subjects in bold are in the interval age between 66 and 72 years.*

Only 20 subjects, divided in 11 HC and 9 MCI, lied in the age intersection between the two age groups (66 to 72 years old). Firstly, we analysed the entire datasets, subsequently we analysed the reduced datasets limited only to the 20 subjects in the intersection of age groups.

3.2.1 Analysis of Entire Datasets

Mann Whitney U Test

We analysed the datasets using the Mann-Whitney test. The p-values are shown in table 3.9; the result is significant at p-value < 0.05.

Graphs

The results showing significant differences are here reported. The couple of mean values of CSA and TAV for each person are shown in graph 3.3 . In blue HC subjects and in red MCI patients.

Mann Whitney U Test	
	p-value
Inflow	0.32
IJV Flow	0.62
Mean CSA	**0.02**
Mean TAV	**0.01**
a	**0.03**
c	**0.03**
x	**0.03**
v	**0.03**
y	**0.02**

Table 3.9: *Results of Mann Whitney U Test for the entire datasets of healthy control subjects and mild cognitive impairment patients. The significant results are reported in bold.*

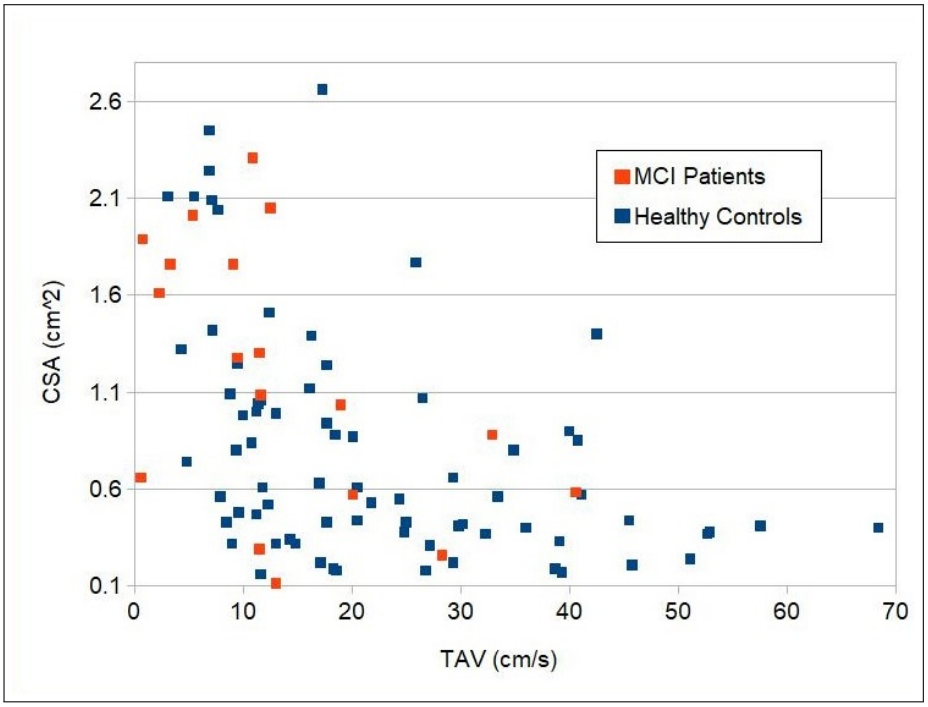

Figure 3.3: *Plot of mean area values (CSA) vs mean velocity values (TAV) for the entire group, each point represent a different subject. In blue healthy control subjects, in red mild cognitive impairment patients.*

The JVP details are reported in figure 3.4, at the bottom the nominal curve, at the top the measured curves with the values averaged between every subject of a group: In blue the HC curve, in red the MCI curve. On every value we draw its standard deviation.

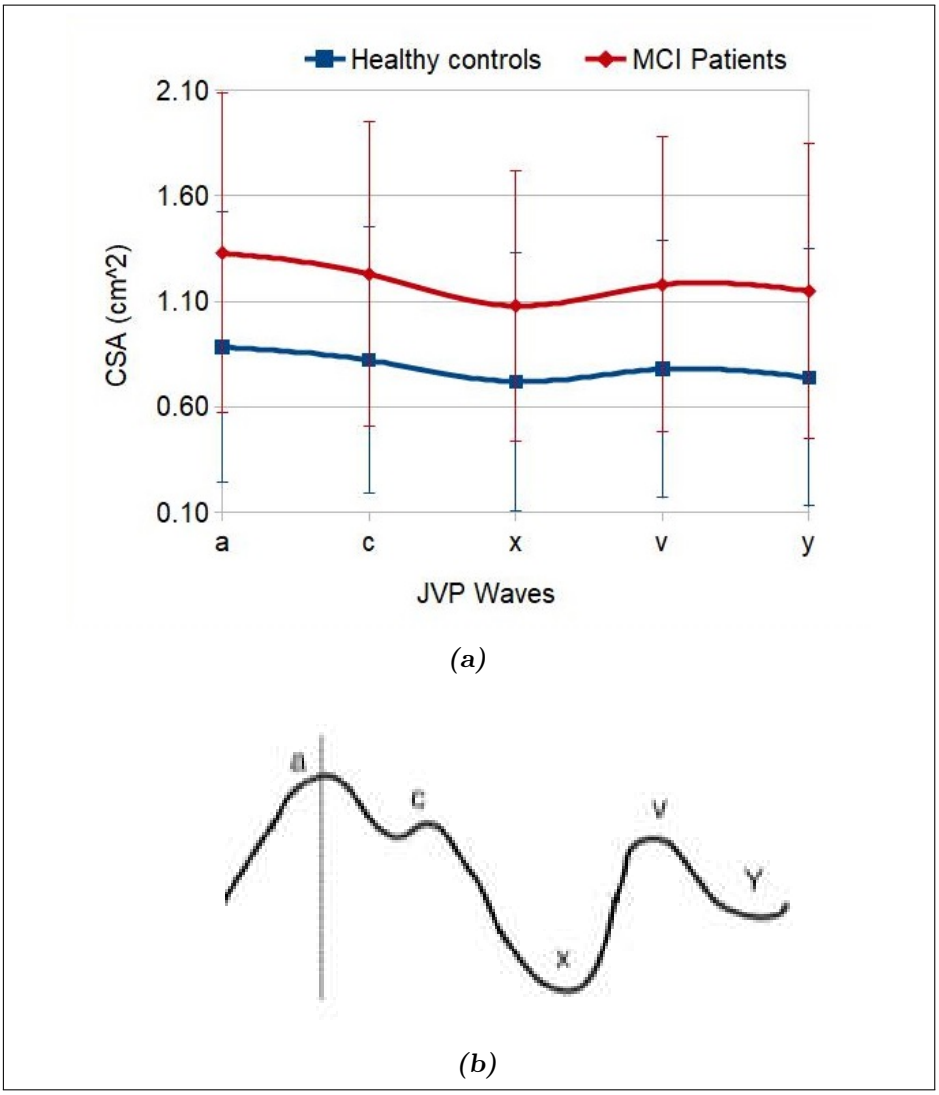

Figure 3.4: *Jugular venous pulse (JVP) details (a, c, x, v, y) are plotted in figures. Figure (b) shows the trace described in literature, figure (a) shows the mean measured details: in blue the details of healthy control subjects, in red the details of mild cognitive impairment patients. On every value is reported its standard deviation.*

Principal Component Analysis

Finally we studied the samples with the PCA selecting CSA, TAV and Age as variables of the study. The results are shown in graph 3.5. In blue HC subjects and in red MCI patients.

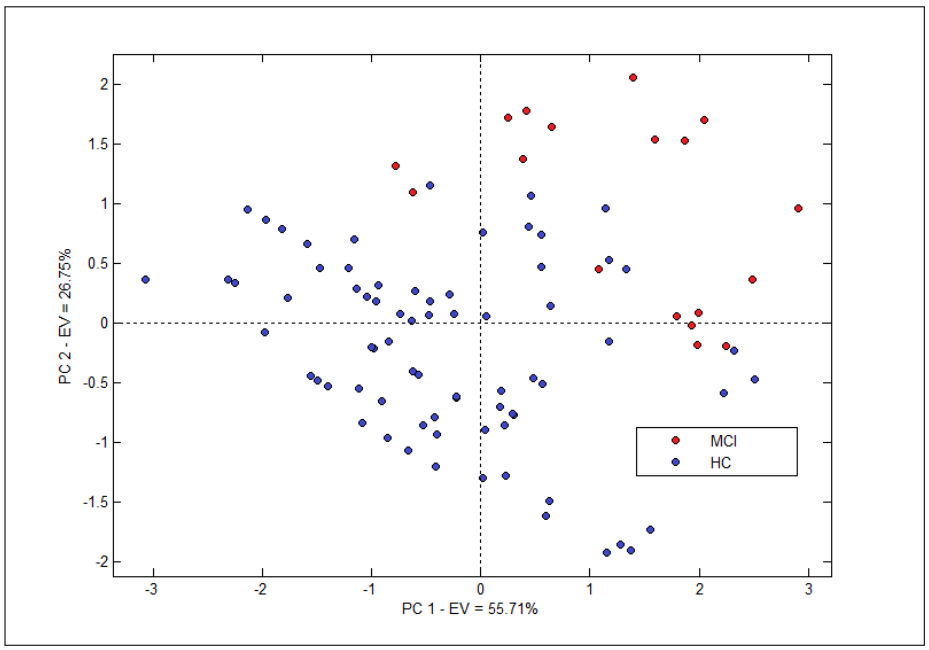

Figure 3.5: *Plot of the Principal Component Analysis results for the entire group. PC1 and PC2 are the two principal component individuated with the analysis. Each point represent a different subject: in blue healthy control subjects (HC), in red mild cognitive impairment patients (MCI).*

3.2.2 Analysis of Reduced Datasets

Mann Whitney U Test

We analysed the reduced datasets using the Mann Whitney U test. The p-values are shown in table 3.10; the result is significant at p-value < 0.05.

Graph CSA vs Mean TAV

We reported in figure 3.6 the couple of mean values of CSA and TAV for each person. In blue HC subjects and in red MCI patients.

Mann Whitney U Test	
	p-value
Inflow	0.51
IJV Flow	1.00
Mean CSA	0.50
Mean TAV	0.60
a	0.76
c	0.70
x	0.52
v	0.70
y	0.50

Table 3.10: *Results of Mann Whitney U Test for the datasets of healthy control subjects and mild cognitive impairment patients reduced to the subjects with an age between 66 and 72 years.*

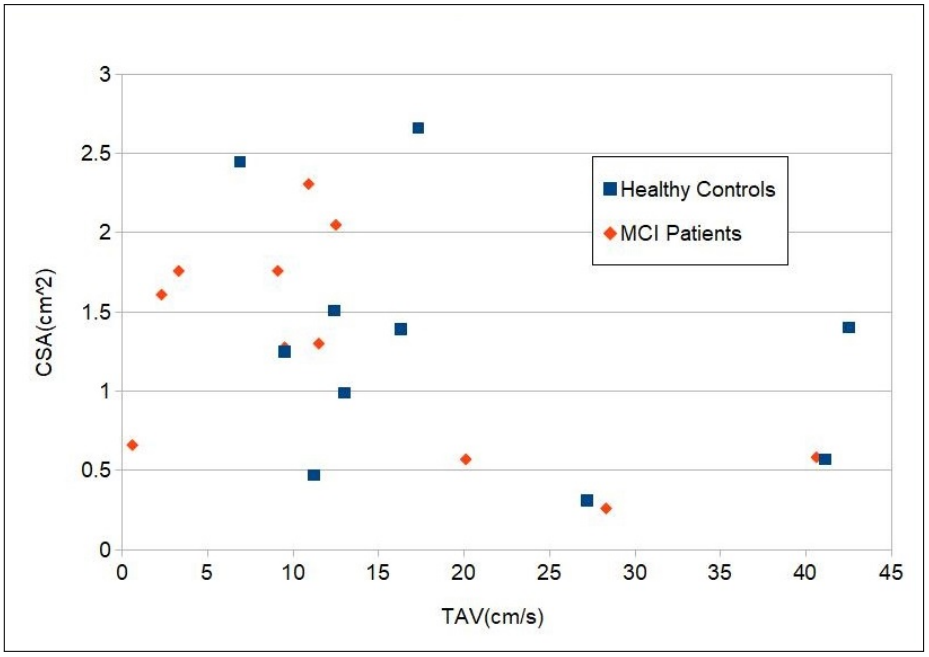

Figure 3.6: *Plot of mean area values (CSA) vs mean velocity (TAV) for each subject with an age between 66 and 72 years. In blue healthy control subjects, in red mild cognitive impairment (MCI) patients.*

Principal Component Analysis

Finally we studied the samples with the PCA selecting CSA, TAV and Age as variables of the study. The results are shown in graph 3.7. In blue HC subjects and in red MCI patients.

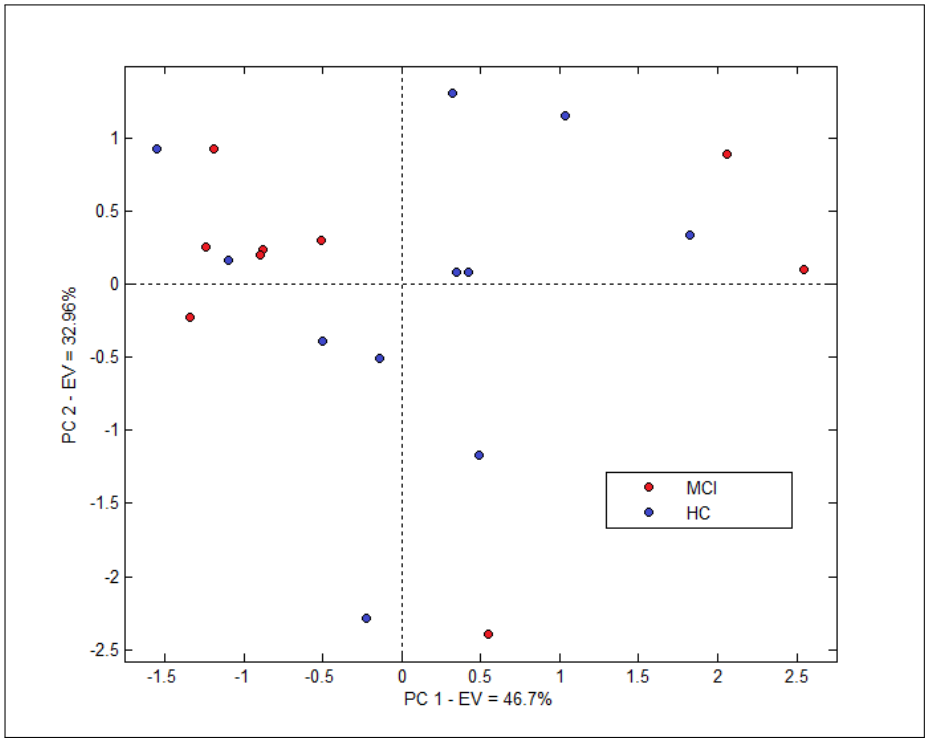

Figure 3.7: *Plot of the Principal Component Analysis results for subjects with an age between 66 and 72 years. PC1 and PC2 are the two principal component individuated with the analysis. Each point represent a different subject: in blue healthy control subjects (HC), in red mild cognitive impairment patients (MCI).*

3.2.3 Analysis of Reduced Datasets Without Outliers

Considering the PCA results of the reduced group (Figure 3.7), 3 MCI patients seem to be outliers. We isolated these subjects and repeated the analysis.

Mann Whitney U Test

Mann Whitney U test was applied to the datasets and the obtained results are shown in table 3.11. The result is significant at p-value < 0.05.

Mann Whitney U Test	
	p-value
IJV Flow	0.80
Mean CSA	0.08
Mean TAV	**0.02**
a	0.14
c	0.14
x	0.17
v	0.17
y	0.14

Table 3.11: *Results of Mann Whitney U test for the datasets of healthy control subjects and mild cognitive impairment patients reduced to the subjects in the age interval between 66 and 72 years without outliers. Significant results are highlighted in bold.*

Graph CSA vs Mean TAV

Then we reported in graph 3.8 the couple of means values of CSA and TAV for each person.

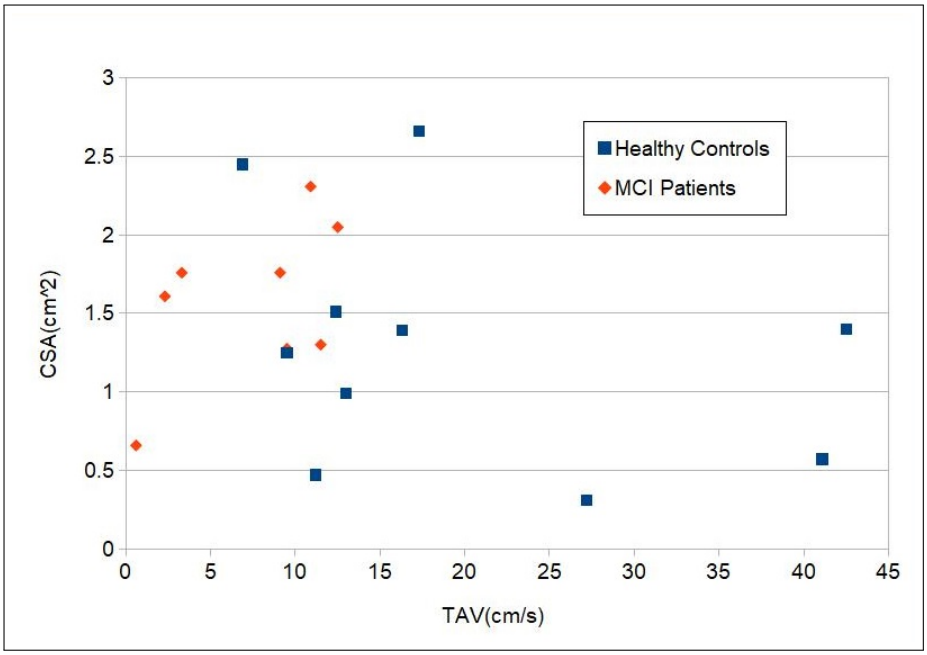

Figure 3.8: *Plot of mean area values (CSA) vs mean velocity (TAV) for each subject in the age interval between 66 and 72 years without outliers. In blue healthy control subjects (HC), in red mild cognitive impairment patients (MCI).*

3.3 JVP vs CVP Project

For the $JVPvsCVP$ project we analysed 60 patients. Since 25 subjects had incomplete examinations or abnormalities in physiological parameters, only 35 subjects were inserted in this study. For every patient we recorded and analysed JVP, of right IJV, and CVP traces (example in figure 3.9). For the last 9 patients (recognisable with a V in the ID), we recorded also the velocity trace.

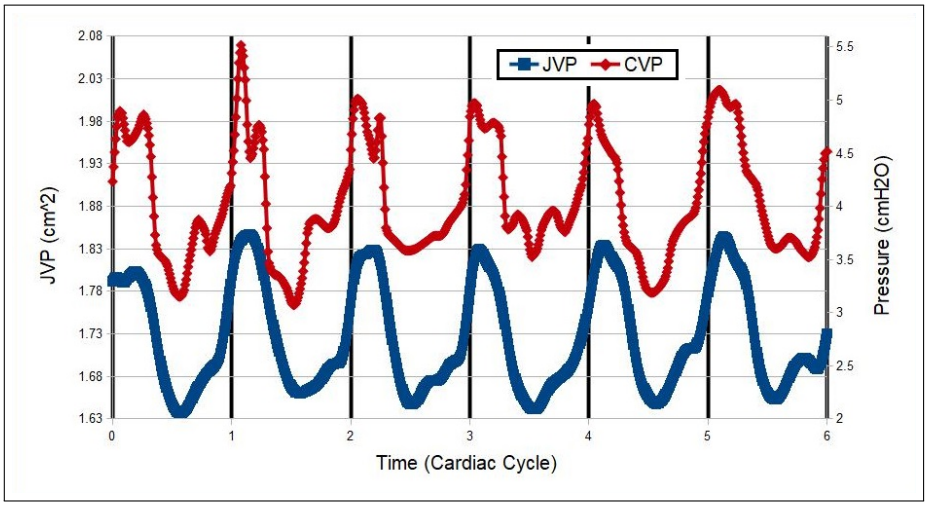

Figure 3.9: *Example of jugular venous pulse (JVP) and central venous pressure (CVP) traces of the same subject.*

Cross correlation analysis was applied to the pair of traces of each subject, recording the maximum correlation and the respective lag. In table 3.12, stored and analysed data are reported together with cross correlation results: CSA mean value and standard deviation, CVP mean value and standard deviation, cross correlation maximum coefficient (r) and LAG in FCC. The maximum r value of cross correlation for each person is even shown in figure 3.10.

Values of MTD between the CVP and JVP traces were calculated as described in section 2.4. In table 3.13 are reported the mean delays of each detail a,c,x,v,y considering the R peak of ECG as zero. The delay of an additional detail, named h, is shown in the same table. These values, quantified in FCC, were calculated for both the JVP and CVP traces.

JVP vs CVP Dataset						
Data	**JVP**		**CVP**		**Cross Correlation**	
ID	**Mean**	**SD**	**Mean**	**SD**	**Max r**	**LAG**
	cm^2		**cmH2O**			**FCC**
1	1.73	0.06	4.0	0.6	90%	3%
4	0.19	0.04	4.0	2.2	67%	26%
5	1.62	0.10	10.9	0.7	76%	9%
8	0.27	0.01	2.0	1.4	39%	-13%
10	1.50	0.10	10.4	0.7	61%	13%
15	0.36	0.01	1.1	1.5	39%	-22%
18	1.45	0.05	8.0	0.9	59%	26%
19	0.48	0.05	1.5	2.1	63%	17%
20	1.50	0.01	5.4	0.8	38%	49%
23	1.91	0.06	3.6	1.7	38%	22%
24	1.35	0.07	1.9	0.8	30%	-154%
25	0.61	0.04	6.8	1.3	80%	17%
28	1.40	0.07	7.7	1.5	68%	1%
30	0.43	0.08	8.1	1.2	59%	15%
31	1.14	0.04	8.6	1.9	66%	16%
34	0.42	0.06	7.3	1.0	65%	12%
38	0.97	0.04	4.2	1.1	79%	-73%
39	0.52	0.02	10.8	1.1	60%	-158%
40	1.68	0.11	7.5	1.1	65%	-176%
42	0.55	0.06	5.4	2.0	76%	17%
44	0.45	0.02	2.6	1.0	62%	-74%
46	1.26	0.05	8.0	1.2	55%	-83%
47	0.96	0.01	6.5	1.4	68%	40%
48	0.27	0.03	2.0	0.7	83%	27%
49	1.22	0.02	4.0	1.6	67%	-82%
50	1.29	0.08	9.0	1.7	59%	28%
V1	0.92	0.03	10.5	0.7	68%	7%
V2	0.62	0.10	3.4	1.6	77%	-81%
V3	1.08	0.05	8.9	0.6	66%	22%
V4	0.89	0.02	8.5	1.3	34%	14%
V5	1.27	0.10	7.1	0.7	87%	13%
V6	1.37	0.09	7.1	1.0	53%	5%
V7	0.45	0.05	3.9	1.1	71%	14%
V8	1.37	0.06	4.4	1.4	39%	-85%
V9	1.06	0.02	7.5	0.6	28%	-72%

Table 3.12: *Jugular Venous Pulse (JVP) and Central Venous Pressure (CVP) Dataset: ID, Mean values and standard deviation (SD). Cross Correlation Results: maximum correlation (Max r) and LAG between the traces.*

Delays of JVP and CVP Details												
ID	**JVP**						**CVP**					
	a	**c**	**x**	**v**	**y**	**h**	**a**	**c**	**x**	**v**	**y**	**h**
	FCC(%)						**FFC(%)**					
1	17	29	59	81	87	-	9	24	54	74	84	-
4	18	44	70	87	91	-	-7	20	40	65	78	-
5	10	24	43	64	78	-	7	13	27	48	68	-
8	48	76	110	114	118	-	-2	24	33	55	74	87
10	12	32	52	72	85	-	-3	13	25	49	72	80
15	51	61	74	94	128	-	-8	17	30	41	53	69
18	26	45	62	72	83	108	-3	14	30	46	60	75
19	21	42	59	74	91	115	1	20	32	56	70	80
20	55	76	94	106	121	135	1	21	30	44	53	71
23	20	35	57	73	84	106	-7	13	23	52	66	78
24	46	70	101	117	122	132	-5	16	30	48	75	83
25	16	31	54	74	90	-	-3	13	33	57	75	-
28	-3	16	40	61	70	81	-4	14	35	52	66	78
30	3	18	48	63	75	-	-10	8	16	44	53	66
31	19	42	51	62	71	98	0	10	24	49	63	77
34	14	21	38	55	75	85	-4	7	19	44	64	74
38	23	44	59	77	92	112	-11	6	20	54	70	-
39	23	51	71	85	96	-	-6	7	28	61	75	-
40	15	35	50	63	71	94	-6	11	23	48	67	-
42	15	30	45	65	90	-	3	12	22	49	64	75
44	12	29	56	70	87	-	-9	11	21	45	55	-
46	5	17	47	74	81	-	-5	8	22	55	74	-
47	39	53	70	85	104	-	5	16	36	69	81	-
48	29	-	68	-	-	-	-1	-	45	-	-	-
49	15	27	46	68	81	100	-4	6	20	54	68	77
50	12	36	56	81	91	-	-37	-12	1	11	25	-
V1	11	-	44	53	65	87	11	-	24	37	49	81
V2	16	-	50	68	80	-	-3	-	28	51	63	78
V3	16	32	56	70	85	-	-1	12	29	54	69	-
V4	9	29	45	59	74	-	-2	10	18	47	60	78
V5	1	21	50	75	83	-	-13	7	35	56	70	-
V6	6	26	57	76	85	-	12	23	36	60	81	102
V7	13	29	53	77	85	-	2	21	32	62	74	89
V8	53	65	84	110	131	-	38	53	68	101	119	-
V9	46	63	78	90	101	-	-12	2	17	46	65	-
Mean	21	39	60	77	90	104	-2	14	29	52	68	79
SD	16	17	17	16	17	17	11	10	12	14	14	8

Table 3.13: *Mean Delays of jugular venous pulse (JVP) and central venous pressure (CVP) details (a, c, x, v, y, h) for each subject (ID). At the bottom Mean values averaged over the entire group and standard deviations (SD).*

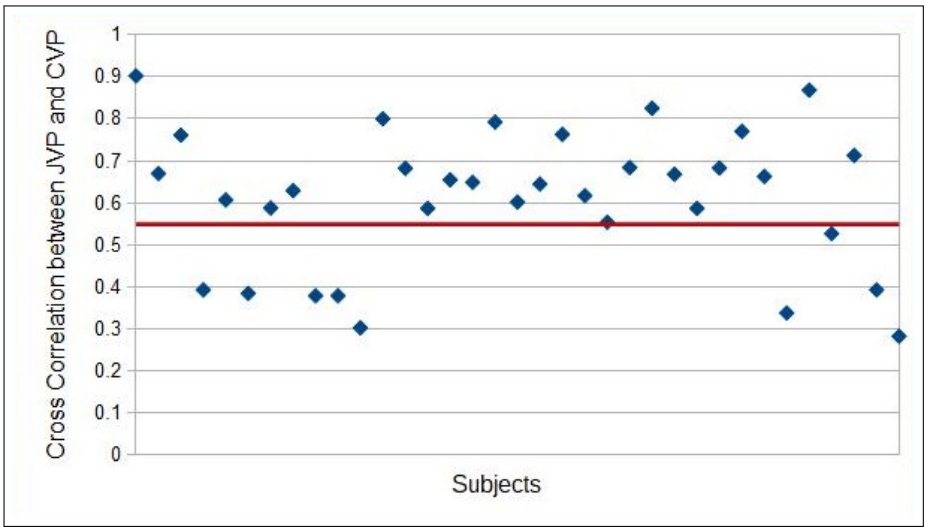

Figure 3.10: *Plot of maximum cross correlation r-value per each subject. Red line represent the 55% of maximum cross correlation between Jugular venous pulse (JVP) and central venous pressure (CVP).*

In table 3.14 are shown the averaged values of delays between the details of the traces, considering the a wave as 0.

Averaged Delays of Details

ID	JVP					CVP				
	c-a	x-a	v-a	y-a	h-a	c-a	x-a	v-a	y-a	h-a
	FCC (%)					FCC (%)				
Mean	18	39	56	69	83	16	31	55	70	80
SD	5	8	9	8	6	5	8	9	10	6

Table 3.14: *Averaged values (Mean) and standard deviation (SD) of mean delays between the details (c-a, x-a, v-a, y-a, h-a) of jugular venous pulse (JVP) and central venous pressure (CVP) traces.*

An example of trace with h detail is shown in figure 3.11.

For each subject we calculated a mean compliance value and a predicted pressure as described in section 2.4. We assumed ρ equal to 1.04 kg/m^3, l_G as a constant equal to 18.0 cm, p_0 as a constant equal to 0 $cmH2O$.

MTD, compliance, calculated pressure mean value and standard deviation, together with the CVP mean value and standard deviation are reported for each subject in table 3.15. We assumed the error on CVP measumerents equal to 0.1 $cmH2O$, since it reflects the precision of the operator (section 3.1).

Model to Predict Pressure						
Data	**CVP**		**MTD**	**Compliance**	**Predicted Pressure**	
ID	**Mean SD cmH2O**		**Mean FCC**	**Mean cm^2/cmH2O**	**Mean SD cmH2O**	
1	4.0	0.6	5%	0.014	119.8	4.4
4	4.0	2.2	23%	0.023	8.6	1.7
5	10.9	0.7	11%	0.056	29.2	1.7
8	2.0	1.4	56%	0.231	1.2	0.0
10	10.4	0.7	19%	0.145	10.4	0.7
15	1.1	1.5	55%	0.076	1.1	0.0
18	8.0	0.9	28%	0.326	4.5	0.1
19	1.5	2.1	22%	0.063	7.7	0.8
20	5.4	0.8	61%	1.589	0.9	0.0
23	3.6	1.7	24%	0.317	6.0	0.2
24	1.9	0.8	59%	1.251	1.1	0.1
25	6.8	1.3	18%	0.055	11.1	0.7
28	7.7	1.5	5%	0.008	181.4	9.3
30	8.1	1.2	19%	0.033	12.7	2.4
31	8.6	1.9	20%	0.122	9.3	0.3
34	7.3	1.0	15%	0.024	17.7	2.4
38	4.2	1.1	31%	0.261	3.7	0.1
39	10.8	1.1	32%	0.148	3.5	0.1
40	7.5	1.1	18%	0.150	11.2	0.8
42	5.4	2.0	19%	0.053	10.4	1.0
44	2.6	1.0	26%	0.088	5.1	0.2
46	8.0	1.2	14%	0.065	19.3	0.7
47	6.5	1.4	29%	0.234	4.1	0.0
48	2.0	0.7	26%	0.046	5.9	0.6
49	4.0	1.6	18%	0.117	10.4	0.1
50	9.0	1.7	58%	1.127	1.1	0.1
V1	10.5	0.7	13%	0.045	20.2	0.7
V2	3.4	1.6	19%	0.049	12.7	2.1
V3	8.9	0.6	19%	0.114	9.4	0.4
V4	8.5	1.3	17%	0.069	13.0	0.4
V5	7.1	0.7	15%	0.072	17.8	1.3
V6	7.1	1.0	11%	0.048	28.3	1.9
V7	3.9	1.1	13%	0.020	22.8	2.6
V8	4.4	1.4	14%	0.061	22.4	1.0
V9	7.5	0.6	74%	0.821	1.3	0.0

Table 3.15: *Dataset of model to predict pressure: ID, central venous pressure (CVP), Mean Time Delay (MTD) between jugular venous pulse and CVP traces, Compliance value, calculated pressure (Calc. Pressure).*

The value of MTD averaged over the entire group is (27 ± 17) % FCC.

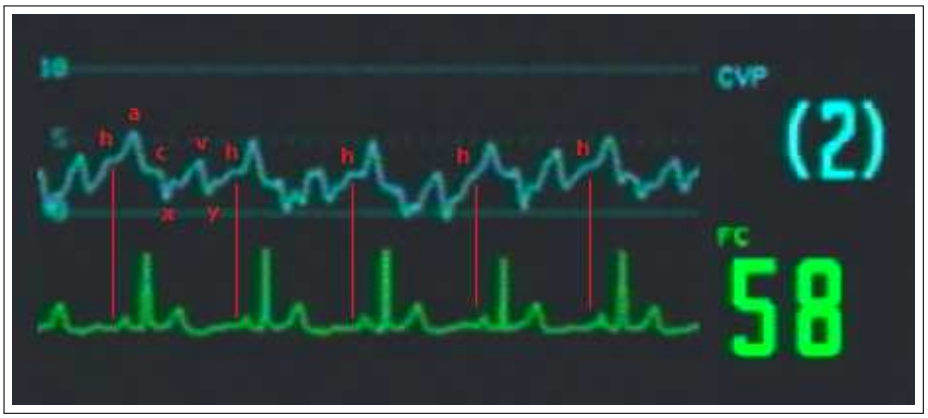

Figure 3.11: *Example of central venous pressure (CVP) trace with h detail and relation with the electrocardiogram trace (Cardiac Frequency, FC).*

Considering the results and knowing that the normal venous pressure is around 4-12 $cmH2O$ [35, 40, 72, 85], the two subjects (ID 1 and 28), with a predicted pressure higher than 100 $cmH2O$, are considered outliers.

For the subjects with stored velocity traces, we calculated also the difference between CVP, measured in vena cava, and calculated pressure in internal jugular vein (see section 2.4); the results are reported in table 3.16.

Pressure differences	
ID	**Delta P cmH2O**
V1	0.046
V2	0.238
V4	0.158
V5	0.109
V6	0.105
V7	0.666
V8	0.089
V9	0.116

Table 3.16: *Difference in pressure (Delta P) per subject (ID) between central venous pressure measured in vena cava and calculated pressure in internal jugular vein.*

Linear Fit

The pairs of values mean CVP and mean predicted pressure are plotted in graph 3.12 together with a linear fit.

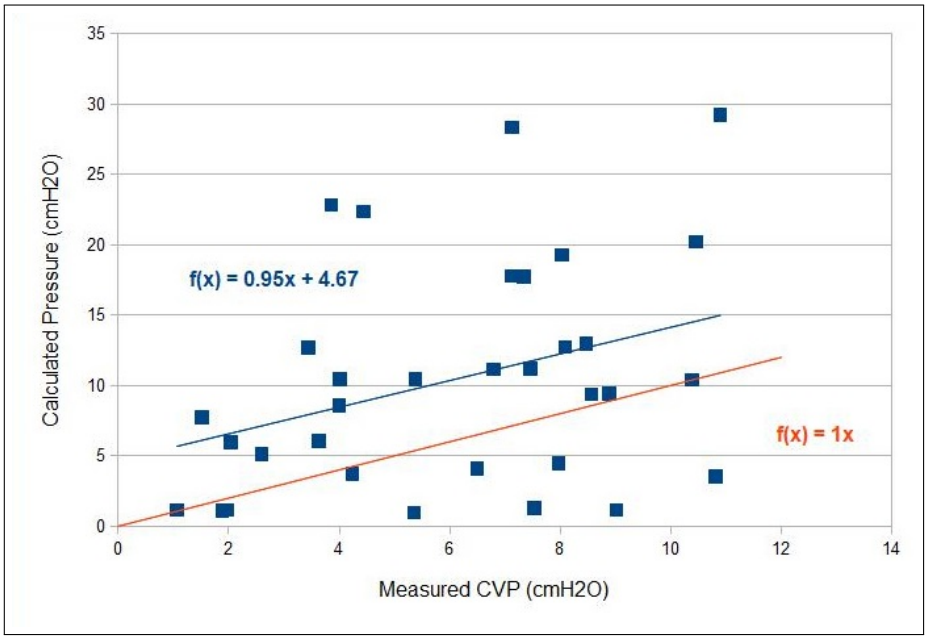

Figure 3.12: *Plot of pairs of values Measured central venous pressure (CVP) and Predicted Pressure, for each subject without the outliers. The blue line is the linear fit on the values, the red line is the ideal linear fit.*

Slope and intercept of the linear fit are 0.95 and 4.67, respectively.

Receiver Operating Characteristic Curve

The Receiver Operating Characteristic (ROC) curves were calculated considering two different thresholds for individuating subjects with normal pressure. The obtained graphs are reported in figure 3.13 *a* and *b*.

There is no general agreement in considering the normal range of CVP [35, 40, 72, 85]. For this work we considered as normal firstly CVP measurements over 4 $cmH2O$, and subsequently CVP measurements below 8 $cmH2O$.

The area under the ROC curve with the threshold at 4 $cmH2O$ is 67%. The area under the ROC curve with the threshold at 8 $cmH2O$ is 65%.

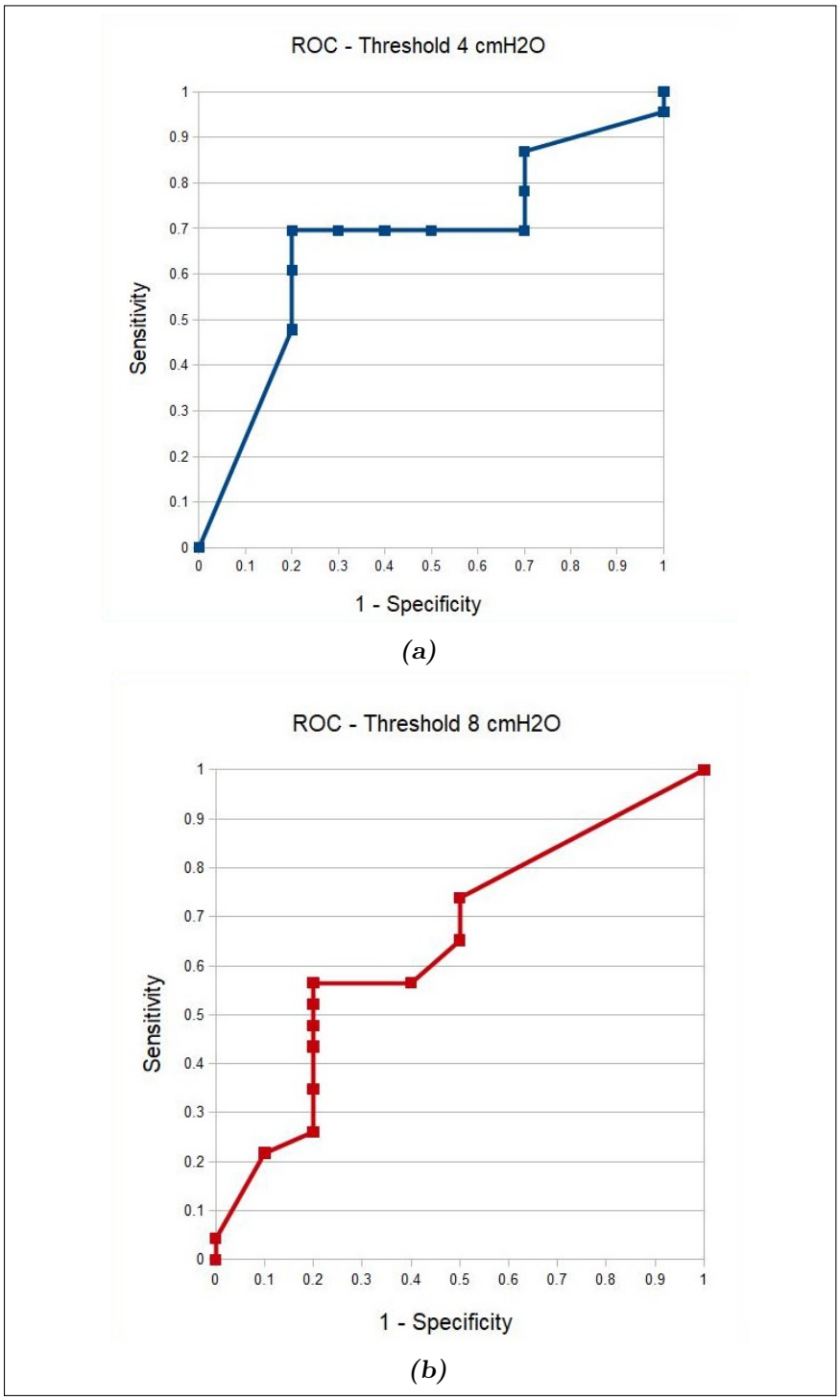

Figure 3.13: *Plot of the receiver operating characteristic (ROC) curve for the model to predict pressure with the threshold of normal central venous pressure equal to 4 cmH2O (a) and equal to 8 cmH2O (b).*

3.4 ULA-OP

3.4.1 Doppler Mode

Reproducibility and Repeatability test were applied. The obtained results, expressed as range of COV are reported in table (3.17).

Repeatability and Reproducibility Test	
TEST	**Range of COV**
Repeatability Std. Device	1-2
Reproducibility Std. Device (sugg. setup)	7-12
Reproducibility Std. Device (best setup)	0-5
Repeatability ULA-OP	7-15
Reproducibility ULA-OP	13-17

Table 3.17: *Results of Repeatability and Reproducibility test on Standard Device with suggested setup and best setup and on ULA-OP platform.*

The results of paired t-test between nominal and measured values collected with ULA-OP and standard device with both the experimental setups are reported in table 3.18. The p-value threshold for statistical significance is 0.05.

Doppler Comparison	
Paired t-test	**p-value**
Std. Device (sugg. setup) - Nominal values	$< \mathbf{10^{-3}}$
Std. Device (sugg. setup) - ULA-OP	$< \mathbf{10^{-4}}$
Std. Device (best setup) - Nominal values	$< \mathbf{10^{-5}}$
Std. Device (best setup) - ULA-OP	$< \mathbf{10^{-2}}$
ULA-OP - Nominal values	> 0.8

Table 3.18: *Results of T-test between Nominal values, Standard Device, with suggested and best setup, and ULA-OP measurements. The significant results are reported in bold.*

Mean measured values are plotted in graph 3.14 together with a linear fit for every device and setup. Slope and intercept of every regression are reported in table 3.19.

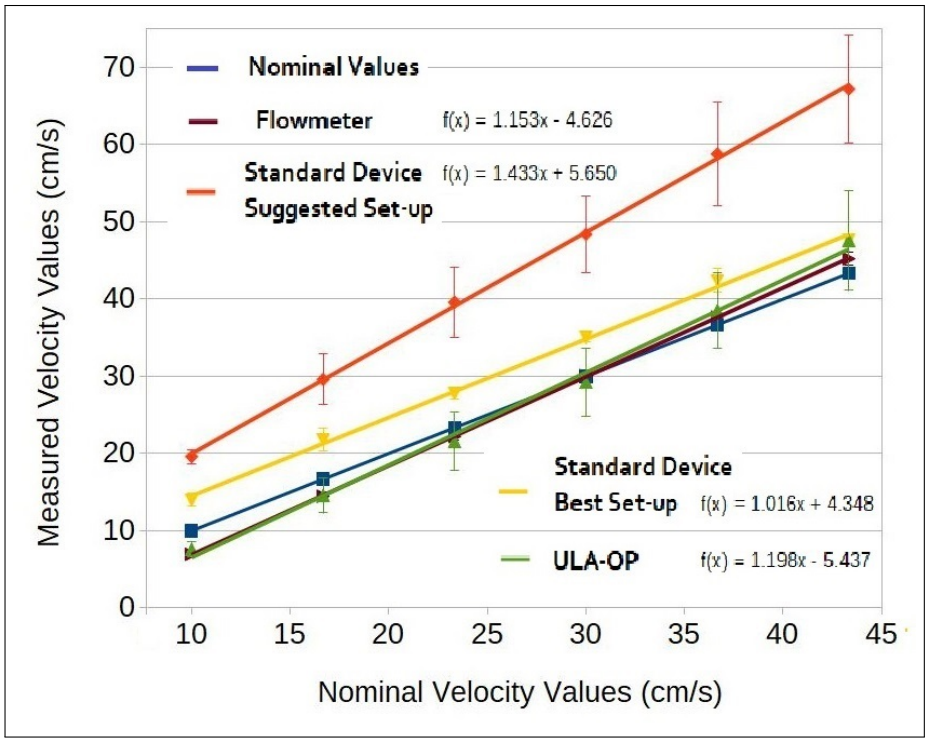

Figure 3.14: *Plot of nominal velocity values vs mean measured velocity values. In blue the nominal values, in purple the flowmeter measurements, in red the standard device measurement obtained with suggested setup, in yellow the standard device measurements obtained with best setup, in green the ULA-OP measurements. Over each data it is drawn the respective linear fit.*

Parameters of Linear Fit			
Device	**Slope**	**Intercept**	**R^2**
Flowmeter	1.153	4.626	1.000
Std Device (sugg. setup)	1.433	5.650	0.999
Std Device (best setup)	1.016	4.348	0.998
ULA-OP	1.198	5.437	0.995

Table 3.19: *Slope, Intercept and R^2 of each linear fit on the datasets of measured values, obtained with Flowmeter, Standard Device with suggested and best setup and ULA-OP.*

3.4.2 Brightness Mode

For the B-mode we used cross correlation and Pearson correlation to compare the JVP traces of 8 healthy subjects. The results are shown in table (3.20).

B-mode Comparison		
ID	**Cross Corr.**	**Pearson Corr.**
01	92%	93%
02	91%	91%
03	60%	63%
04	86%	82%
05	90%	94%
06	76%	78%
07	81%	82%
08	81%	83%

Table 3.20: *Results of Cross Correlation and Pearson Correlation between pairs of jugular venous pulse traces obtained, for each subject (ID), with ULA-OP and standard device.*

Finally the SdNR test results are for the ULA-OP device 3.8, for the standard device 45.8.

4 Discussion

At the beginning of this thesis work we verified, with a quality control process, the good level of performance of the US device used during the experimental sections on subjects. The experimental projects, set up in parallel way in this work, were the "HC vs MCI" and the "JVP vs CVP".

The "HC vs MCI" project has been conducted in outpatient clinic using non-invasive US technology. The evaluated hemodynamic parameters were: arterial blood inflow to the brain, IJV CSA and blood velocity and JVP waves. The off-line post processing was done using the Mann Whitney U test and the PCA. Firstly, studying the entire populations, we verified that CSA and velocity values of MCI patients are statistically different with respect to HC subjects ($p-value_{CSA} = 0.02$ and $p-value_{TAV} = 0.01$), as predicted in literature [12–17]. Then, reducing the number of studied subjects to avoid any sort of bias due to the different range of age of the populations [86], we found that CSA and TAV values of MCI and HC subjects are less significant different ($p-value_{CSA} = 0.08$ and $p-value_{TAV} = 0.02$), or even not different at all ($p-value_{CSA} = 0.50$ and $p-value_{TAV} = 0.60$).

The "JVP vs CVP" project has been executed on surgical patients, recording CVP measurements via a CVC and US examination simultaneously. For the off-line post processing we used Cross Correlation, Linear Fit and ROC Curve. Firstly, we verified that CVP and JVP traces of the same subjects are correlated ($r_{max} > 55\%$ in 26/35 subjects), as predicted in literature [34, 40–42, 49], and we quantified a mean time delay between the traces. Then, following a model described in literature [9–11, 31, 52, 53], we found an experimental way to predict pressure values starting from CSA measurements. The results are currently weak ($ROC_4 = 67\%$ and $ROC_8 = 65\%$) but promising for future improvements of the model.

Finally, we studied the ULA-OP system making a comparison with the performance of a standard device. The test was done for both the Doppler and the B-mode, in-vitro and in-vivo respectively. The comparison was analysed with the Student T test and Cross Correlation. As regard the quantification of blood velocity, we studied precision and accuracy of measurements of the ULA-OP, comparing the obtained measurements to the ones of the standard devices and to the nominal values. The results shows that ULA-OP has higher accuracy ($p - value_{ULA-OP} > 0.8$, $p - value_{StdDev} <$ 10-3), but lower precision than the standard device (Repeatability COV_{ULA-OP} = 7-15, COV_{StdDev} = 1-2; Reproducibility COV_{ULA-OP} = 13-17, COV_{StdDev} = 0-5). On the other hand, for the B-mode representation we compare the performances of the two devices considering the standard device as the reference point. The obtained measurements are very similar between the devices ($r_{max} > 76\%$ in $7/8$ subjects).

In the following discussion each argument is developed in detail.

4.1 Quality Control Test

Considering the repeatability results, the precision of the operator is equal to the precision of the device. Therefore, the uncertainty carried by the operator can be considered negligible.

The uniformity of the signal (Table 3.2) is better at the maximum frequency. On the contrary the depth of penetration (Table 3.3) is better at the minimum frequency.

The dead zone is smaller than the threshold of precision of the device.

The beam profiles (Figure 3.1) are similar to the nominal one, considering that the precision of the US device reported by the manual (Table 3.1) is larger than the differences between the measurements.

Vertical (Table 3.4) and horizontal measurements are equivalent to the nominal values.

Axial and Lateral Resolution (Figure 3.2) are equal to the minimum distance measurable with the phantom.

The diameter measurements, both in horizontal and vertical direction, both of anechoic (Table 3.5) and grey scale cylinders (Table 3.6), are not significantly different from the nominal values.

In conclusion the performance level of the US device is optimal, since the measurements on the phantom are consistent with the nominal values.

4.2 HC vs MCI Project

4.2.1 Analysis of Entire Datasets

Considering the Mann Whitney U test results (Table 3.9), arterial inflow and IJV flow between the two populations are not significantly different. On the contrary, IJV CSA, TAV and JVP details are significantly different.

As shown in figure 3.3, MCI patients generally have larger CSA values and lower velocities than HC subjects. This is in accordance with the equivalence of IJV flow values between the two populations.

Moreover, JVP details are larger in MCI patients than in HC subjects (Figure 3.4).

Analysing the PCA graph (Figure 3.5), two groups of subjects are detectable. More than 72% of MCI patients are in the upper right part of the figure. On the contrary, the HC subjects are almost equally divided in the whole graph.

4.2.2 Analysis of Reduced Datasets

In this case, the Mann Whitney U test (Table 3.10) verified that no parameters are significantly different.

As shown in the figure 3.6, both populations have subjects with both large and small CSA, and high and low velocities.

Considering the PCA (Figure 3.7), almost the 67% of MCI subjects are in the upper left part of the graph. The other 3 MCI patients are rather far from this group and could be considered as outliers. HC subjects are almost equally divided in the whole graph.

4.2.3 Analysis of Reduced Datasets Without Outliers

Excluding the outliers from the MCI population, the significance levels obtained with the Mann Whitney U test increase. However, these levels (with the sole exception of mean TAV) remain higher than the selected threshold: therefore, almost no parameters are statistically different.

Regarding the graph (3.8), MCI patients generally have larger CSA values and lower velocities than HC subjects.

To summarize, the obtained results are good: the statistical differences among the entire populations of HC and MCI subjects, predicted in the literature [12–16], were verified by our study. As a matter of fact, the results could be affected by a bias, since the populations have different range of age, a factor which could influence the measurements [86]. Indeed, the

statistical differences between the populations reduced to the same range of age vanished almost completely. It is worth noting, that statistical tests on the reduced datasets have a low level of robustness, since the number of subjects is rather small. For the future, it is preferable to increase the dataset with subjects in the same range of age, in order to have a larger statistic.

If the future results confirmed the statistical difference in CSA and TAV between the two populations, JVP analysis and velocity measurement could be considered as a preliminary diagnostic method for MCI.

4.3 JVP vs CVP Project

Considering cross correlation results (Table 3.12), 26 subjects out of 35 have the maximum r of cross correlation higher than 55%. It means that the traces are related as described in paragraph (*1.3*). Regarding the LAG, it can be positive or negative depending on which trace is moving with respect to the other. Obviously, absolute values of the LAG >100% of FCC implicate that one or more cardiac cycles (of JVP or CVP) were excluded from the cross correlation.

The comparison between the delays of the last five details with respect to the delays of the first one, calculated in table (3.14), shows that JVP and CVP traces have almost the same time lags.

The h wave, generally not described in literature, is detectable in 60% of the population and corresponding to the beginning of the P wave of the ECG (Table 3.13 and Figure 3.11).

As shown in the table 3.15, the MTD averaged over the entire population is equal to a quarter of cardiac cycle ± 17% FCC. The compliance value is quantified between 0.014 and 0.326 $cm^2/cmH2O$ for almost 86% of the analysed subjects.

The mean difference between CVP and predicted pressure is negligible, since it is in the same order of magnitude of the error on CVP measurements.

Analysing the linear fit over the model results (Figure 3.12), the slope of the regression is very close to the one of the ideal fit; on the contrary, the intercept is bigger than the ideal one.

Finally, the area measurements under the ROC curves are quite similar: the predicted performance of the ROC with threshold equal to 4 cmH2O is slightly larger (67%) than the one of the ROC with the threshold of 8 cmH2O (65%).

In this work, we verified the correlation between JVP and CVP traces. We quantified a mean delay between the entire traces and between each detail. Moreover, we found out that most of the analysed subjects showed the h wave in JVP or CVP trace. Finally, we applied a model to predict pressure values using measurements of CSA and compliance values. The performances of the model, that is at its first practical implementation, are currently weak but promising for future improvements. For example, a deeper study on the distance between the two points of measurement could be very helpful. We preferred to use a constant length to avoid other invasive analysis, however an error on this parameter of only $\pm$ 2 cm would cause a variation of about 25% on the predicted pressure. The result could be largely influenced also by the addictive constant pressure p_0, here assumed equal to 0 cmH2O: also this parameter could be examined in depth in further studies.

The final goal is to improve the model in order to quantify the venous pressure only examining a US JVP trace and avoiding invasive measurements.

4.4 ULA-OP

4.4.1 Doppler Mode

Considering repeatability and reproducibility results shown in Table (3.17), the standard device has a better repeatability and reproducibility than the ULA-OP.

Regarding the t-test results shown in the table (3.18), the ULA-OP has a better performance than standard devices in estimating velocity.

The linear fit (Figure 3.14 and Table 3.19) confirmed that the ULA-OP measurements are more accurate than the standard device's ones: ULA-OP values are closer to the flowmeter measurements than standard device quantifications.

In conclusion, the ULA-OP shows higher accuracy, but lower precision than the standard device. Probably, the low precision is related to the display mode of the measurements. The standard device displays a TAV value calculated in a certain time frame, whereas the ULA-OP shows a single velocity measurement that is continually refreshed. We think that the user interface of the ULA-OP has to be improved showing also the TAV value, in order to consider the system for the clinical environment.

4.4.2 Brightness Mode

As shown in table (3.20), the results of cross correlation between the trace recorded with ULA-OP and standard device are very high. Every subject has a correlation between 60% and 92%.

Moreover, considering the Pearson correlation, the results are even higher: Between 63% and 94%. It means that the trace are linearly related.

Considering that traces were stored within a few minutes of each other, and probably not in the very exact position along the IJV, a little difference between the traces is acceptable.

For these reasons, we can state that the B-mode performances of both devices are very similar.

Regarding the SdNR, the performance of ULA-OP is worse than standard device's ones, since the software system of the second device probably automatically applies some filters to the images.

To summarize, in order to use the ULA-OP device in medical diagnostics, it will be necessary to store a millimetre scale on the images to measure CSA in cm^2. Moreover, it is preferably to increase the SdNR of the image by applying some sort of filtration during the elaboration of the data.

Once the improvements were applied, the ULA-OP could be ready for clinical use. The ULA-OP characteristics could raise the level of accuracy of Doppler US measurements of velocity. Moreover, novel custom functionalities could be implemented at the software level of the ULA-OP system: this improvements would be useful for different research fields.

Conclusions

The aim of this thesis work was to accomplish two projects related to clinical examinations about Mild Cognitive Impairment (MCI) and venous pressure, respectively. The standard Ultrasound (US) device used to perform this examinations was carefully tested by using a dedicated phantom. Moreover, advanced hardware and software tools have been developed and tested in order to overcome current limitations of standard clinical protocols.

Once verified that the performances of the selected US device are optimal for vascular examinations, we completed the two projects in parallel ways.

The goal of the first project was to investigate statistical differences in healthy control subjects and MCI patients by comparing their vascular examinations. By using the whole collected datasets, we found statistically differences between the groups. Subsequently, we reduced both groups to the same age interval to avoid bias. In this case the results are not significantly different. However, the robustness of these last tests was very low, since the number of subjects was rather small.

During the second project we verified the intra-subject correlation between Jugular Venous Pulse (JVP) and Central Venous Pressure (CVP) traces. We found a mean delay between the entire traces and between each detail. Beside, the JVP and CVP techniques used in this study allow us to detect the h wave, a detail rarely described in literature, in most of the analysed subjects. Finally we applied a model to predict the venous pressure by using cross sectional area measurements and compliance values. The performances of the model are currently weak but promising for future improvements.

In the last part of this thesis work I characterized an US Advanced Open Platform (ULA-OP) by comparing its performances with the ones of a standard device. The Doppler mode of the ULA-OP shows higher

accuracy but lower precision than the standard device. The Brightness mode performances are very similar for both devices, even if the image quality of the ULA-OP is worse. However, the high programmability of ULA-OP, one of the main innovations of this device, could compensate the defects. Once implemented the necessaries adjustments, this platform could become very useful for cardiovascular diagnostics.

Bibliography

[1] Zamboni P, Galeotti R, Menegatti E, Malagoni A M, Tacconi G, Dall'Ara S, Bartolomei I, Salvi F. **Chronic cerebrospinal venous insufficiency in patient with multiple sclerosis**. J Neurol Neurosurg Psychiatry, 2009;80:392-9.

[2] Gadda G, Taibi A, Sisini F, et al. **A new hemodynamic model for the study of cerebral venous outflow**. Am J Physiol, 2015;308:217-31.

[3] Sisini F, Gianesini S, Menegatti E, Taibi A, Tessari M, Di Domenico G, Malagoni A M, Gambaccini M. **On the consistency of flow rate color Doppler assessment for the jugular vein**. Veins and Lymphatics, 2014. DOI: 10.4081/vl.2014.1863

[4] Sisini F, Tessari M, Menegatti E, et al. **Clinical applicability of assessment of jugular flow over the individual cardiac cycle compared with current ultrasound methodology**. Ultrasound Med Bio, 2016;1-14.

[5] Zamboni P, Sisini F, Menegatti E, Taibi A, Malagoni A M, Morovic S, Gambaccini M. **An ultrasound model to calculate the brain blood outflow through collateral vessels: a pilot study**. BMC Neurology, 2013;13-81.

[6] Sisini F, Tessari M, Gadda G, Di Domenico G, Taibi A, Menegatti E, Gambaccini M, Zamboni P. **An ultrasonographic Technique to assess the jugular venous pulse: a proof of concept**. Ultrasound Med Bio, 2015;41:1334-41.

[7] Sisini F. **Quantitative analysis of jugular venous pulse obtained by using a general-purpose ultrasound scanner**. arXiv:1604.05177v1, physics.med-ph, 2016.

[8] Mackenzie J. **The Study of the Pulse, Arterial, Venous, and Hepatic and of the Movements of the Heart**. Young J Pentland, Edinburgh, Scotland, 1902.

[9] Sisini F, Toro E, Gambaccini M, Zamboni P **The Oscillating Component of the Internal Jugular Vein Flow: The Overlooked Element of Cerebral Circulation** Behavioural Neurology, 2015;2015:1-9.

[10] Sisini F **Physical description of the blood flow from the internal jugular vein to the right atrium of the heart: new ultrasound application perspectives**. arXiv:1604.05171v1, physics.med-ph, 2016.

[11] Zamboni P, Tavoni V, Sisini F, Pedriali M, Rimondi E, Tessari M, Menegatti E. **Venous compliance and clinical implications** Veins and Lymphatics, 2018; 7:7367. DOI: 10.4081/vl.2018.7367 .

[12] Chou CH, Chao AC, Lu SR, Hu HH, Wang SJ. **Cephalic venous congestion aggravates only migraine-type headaches**. Cephalalgia 2004;24:973-979.

[13] Chung CP, Hsu HY, Chao AC, Wong WJ, Sheng WY, Hu HH. **Flow volume in the jugular vein and related hemodynamics in the branches of the jugular vein.** Ultrasound Med Bio, 2007;33:500-505.

[14] Doepp F, Schreiber SJ, Dreier JP, Einhaupl KM, Valdueza JM. **Migraine aggravation caused by cephalic venous congestion**. Headache 2003;43:96-98.

[15] Liu M, Xu H, Wang Y, Zhong Y, Xia S, Utriainen D, Wang T, Haacke E M. **Patterns of chronic venous insufficiency in the dural sinuses and extracranial draining veins and their relationship with white matter hyperintensities for patients with Parkinson's disease**. J. Vasc. Surg.,2014.

[16] Zivadinov R, Chung C P. **Potential involvement of the extracranial venous system in central nervous system disorders and aging** BMC Medicine, 2013;11:260

[17] Beggs C, Chung C P, Bergsland N, Wang P N, Shepherd S, Cheng C Y, Dwyer M G, Hu H H, Zivadinov R. **Jugular venous reflux and brain parenchyma volumes in elderly patients with mild cognitive impairment and Alzheimer's disease** BMC Neurology, 2013;13:157

[18] Tortoli P, Bassi L, Boni E, Dallai A, Guifi F, Ricci S. **ULAOP:an advanced open platform for ultrasound research**. IEEE Trans Ultrason Ferroelectr Freq Control 2009;56:2207-16.

[19] Tortoli P, Palombo C, Ghiadoni L, Bini G, Francalanci L. **Simultaneous ultrasound assessment of brachial artery shear stimulus and flow-mediated dilation during reactive hyperemia.** Ultrasound Med Bios, 2011;37:1561-70.

[20] Albinsson J, Hasegawa H, Takahashi H, Boni E, Ramalli A, Ahlgren A R, Cinthio M. **Iterative 2D tissue motion tracking in ultrafast ultrasound imaging** Appl Sci, 2018;8:662.

[21] Herman I P. **Physics of the Human Body**. Springer, 2007.

[22] Furukawa S, Nakagawa T, Sakaguchi I, Nishi K. **The diameter of the internal jugular vein studied by autopsy**. Rom J Leg Med, 2010;2:125-8.

[23] Clark J H. **The elasticity of veins**. American Journal of Physiology, 1933;105:418-27.

[24] Nadiya Y. Mohammed **Study of internal jugular vein valve mechanism function: post analysis of M-mode imaging and an experimental model under cardiac monitoring**. PhD Thesis, 2018.

[25] Zamboni P, Morovic S, Menegatti E, Viselner G, Nicolaides A N. **Screening for chronic cerebrospinal venous insufficiency (CCSVI) using ultrasound–recommendations for a protocol**. Int Angiol,2011;30;6:571-97. Erratum in Int Angiol,2012;31;2:201.

[26] Aplerin N, Lee S, Sivaramakrishnan A, Hushek S **Quantifying the Effect of Posture on Intracranial Physiology in Humans by MRI Flow Studies** Journal of Magnetic Resonance Imaging, 2005;22:591-6.

[27] Starr C, Taggart R. **Biology: The unity and diversity of life**. California: Wadsworth, 1989:398.

[28] Grolier. **New book of popular science**. Connecticut, 1996:197.

[29] O'Neil D. **Blood Components**. Palomar College, California,1999.

[30] **All About Heart Rate (Pulse)** American Heart Association, 2017.

[31] Fung Y C. **Biomechanics:Circulation**. Springer,NewYork,NY, USA,1997.

[32] **https://web.archive.org/web/20080821165806/http://www.healthsystem.virginia.edu/internet/anesthesiology-elective/cardiac/cvcphys.cfm** Anesthesiology Rotation Elective, 2005.

[33] Griffith G C, Chamberlain C T, Kitchell J R. **Observation on the practical significance of venous pressure in health and disease with a review of the literature**. Am J Med Sci 1934; 187: 642-9.

[34] Lewis T. **Early signs of cardiac failure of the congestive type**. Brit Med J, 1930;1:849-52.

[35] Borst J G, Molhuysen J A. **Exact determination of the central venous pressure by a simple clinical method**. Lancet, 1952;2:304-9.

[36] McGee D C, Gould M K. **Preventing complications of central venous catheterization**. New England Journal of Medicine, 2003;348:1123–33.

[37] Bowdle A. **Vascular complications of central venous catheter placement: Evidence-based methods for prevention and treatment.** Journal of Cardiothorac Vascular Anesthesia, 2014;28:358–68.

[38] Vats H S. **Complications of catheters: Tunneled and nontunneled**. Advances in Chronic Kidney Disease, 2012;19:188–94.

[39] Kornbau C, Lee K C, Hughes G D, Firstenberg M S. **Central line complications**. International Journal of Critical Illness and Injury Science, 2015;5(3):170–8.

[40] Siva B, Hunt A, Boudville N. **The sensitivity and specificity of ultrasound estimation of central venous pressure using the internal jugular vein**. J Crit Care, 2012;27:315.

[41] Cook D J, Simel D L. **Does This Patient Have Abnormal Central Venous Pressure?**. Jama, 1996;275:630-4.

[42] Lipton B. **Estimation of Central Venous Pressure by Ultrasound of the Internal Jugular Vein**. Am J Emerg Med, 2000;18:432-4.

[43] Applefeld M M. **The jugular venous pressure and pulse contour**. The history, physical and laboratory examinations. Boston: Butterworths, 1990;19.

[44] Mackay I F S. **An experimental analysis of the jugular pulse in man**. J Physiol, 1947;106:113-8.

[45] O'Rourke R A, Silverman M E, Schlant R C. **General Examination of the Patient**. The heart: arteries and veins. New York: McGraw-Hill,1994:219.

[46] Mancini M, Lanzillo R, Liuzzi R, Di Donato O, Ragucci M, Monti S, Salvatore E, Morra V B, Salvatore M. **Internal jugular vein blood flow in multiple sclerosis patients and matched controls**. PLoS ONE 2014;9:e92730.

[47] Chua Chiaco J M, Parikh N I, Fergusson D J. **The jugular venous pressure revisited.** Cleve Clin J Med, 2013;80:638-44.

[48] Clarke I, Moore L, Veldhuis J. **Intensive direct cavernous sinus sampling identifies high frequency, nearly random pattern of FSH secretion in ovariectomized ewes: Combined appraisal by RIA and bioassay**. Endocrinology, 2002;143:117-29.

[49] Deol G R, Collett N, Ashby A, Schmidt G A. **Ultrasound accurately reflects the jugular venous examination but underestimates central venous pressure**. Chest, 2011;139:95-100.

[50] Drazner M H, Rame J E, Stevenson L W, Dries D L. **Prognostic importance of elevated jugular venous pressure and a third heart sound in patients with heart failure**. N Engl J Med, 2001;345:574-81.

[51] Sahani A K, Shah M, Joseph J, Sivaprakasam M. **Carotid and Jugular Classification in ARTSENS**. JBHI, 2015:1.

[52] Bessems D,Rutten M,VanDeVosse F **A wave propagation model of blood flow in large vessels using an approximate velocity profile function**. Journal of Fluid Mechanics, 2007;580:145–168.

[53] Womerlsey J R **Oscillatory flow in arteries: the constrained elastic tube as a model of arterial flow and pulse transmission** Physics in Medicine and Biology, 1957;2:178–87.

[54] Pyhel H J, Stewart J. **Clinical assessment of calibrated jugular pulse recording.** British Heart Journal, 1978:297-302.

[55] Gill R W. **Measurement of blood flow by ultrasound: accuracy and sources of error**. Ultrasound Med Bio,1985;11:625-41.

[56] Polak J F. **Peripheral Vascular Sonography**. Lippincott Williams Wilkins, 2004;1.

[57] Bushberg J T, Seibert J A, Leidholdt E M, Boone J M. **The essential physics of medical imaging** Lippincott Williams Wilkins,2011.

[58] Tavoni V. **Clinical Applicability of an US model to calculate the head blood outflow through collateral vessels**. Master Thesis

[59] Park M Y, Jung S E, Byun J Y, Kim J H, Joo G E. **Effect of Beam-Flow Angle on Velocity Measurements in Modern Doppler Ultrasound Systems**. American journal of roentgenology, 2012;198:1139-43.

[60] **Manual Phantom, CIRS, Model 054GS, Norfolk, Virginia, USA**

[61] Guidi G, Licciardello C, Faltieri S. **Intrinsic Spectral Broadening (ISB) in ultrasound doppler as a combination of transit time and local geometrical broadening**. Ultrasound in Med. & Biol.,2000;26;5:853-62.

[62] Tortoli P, Guidi G, Newhouse V L. **Improved blood velocity estimation using the maximum Doppler frequency**. Ultrasound in Med. & Biol.,1995;21:527-532.

[63] Menegatti E, Genova V, Tessari M, Malagoni A M, Bartolomei I, Zuolo M, Galeotti R, Salvi F, Zamboni P. **The reproducibility of colour Doppler in chronic cerebrospinal venous insufficienzy associated with multiple sclerosis**. Int Angiol, 2010;29:121-6.

[64] Pickersgill C H, Marr C M, Reid S W. **Repeatability of diagnostic ultrasonography in the assessment of the equine superficial digital flexor tendon**. Equine vet.J., 2001.

[65] Ciccone MM, Galeandro AI, Scicchitano P, et al. **Multigate quality Doppler profiles and morphological/hemodynamic alterations in multiple sclerosis patients.** Curr Neurovasc Res, 2012;9:120-7.

[66] Monti L, Menci E, Piu P, Leonini S, Arrigucci U, Bellini M, Zandonella A, Galluzzi P, Casasco A. **A sonographic quantitative cutoff value of cerebral venous outflow in neurologic diseases: a blinded study of 115 subjects**. Am J Neuroradiol, 2014;35:1381-6.

[67] Thibault P, Lewis W, Niblett S. **Objective duplex ultrasound evaluation of the extracranial circulation in multiple sclerosis patients undergoing venoplasty of internal jugular vein stenoses: a pilot study**. Phlebology, 2015;30:98-104.

[68] Tortoli P, Guidi F, Guidi G, Atzeni C. **Spectral velocity profiles for detailed ultrasound flow analysis**. IEEE Trans Ultrason Ferroelectr, 1996;43:654–9.

[69] Tortoli P, Dallai A, Bassi L, Boni E, Ricci S. **Automatic angle tracking method for dual-beam vector doppler applications**. IEEE Ultrasonics Symp 2008;1056-9.

[70] Tortoli P, Dallai A, Boni E, et al. **An automatic angle tracking procedure for feasible vector Doppler blood velocity measurements**. Ultrasound Med Bio, 2010;36;488-96.

[71] Tavoni V, Sisini F, Di Domenico G, Mohammed N, Gadda G, Calderoni F, Gambaccini M. **Conventional echo color Doppler versus ULA-OP in the assessment of venous flow model** Veins and Lymphatics 2017;6:6841. DOI: 10.4081/vl.2017.6841 .

[72] Cole E. **Measuring central venous pressure**. Nursing Standard, 2007;22:40-2.

[73] Schneider C A, Rasband W S, Eliceiri K W. **NIH Image to ImageJ: 25 years of image analysis**. Nat Methods, 2012;9:671–675.

[74] Cohen A, Ryan R D. **Wavelets and Multiscale Singal Processing**. Chapman and Hall/CRC, 1995.

[75] Taibi A, Gadda G, Gambaccini M, Menegatti E, Sisini F, Zamboni P. **Investigation of cerebral venous outflow in microgravity**. Physiol Meas, 2017;38:1939-52.

[76] Taibi A, Andreotti M, Cibinetto G, Cotta Ramusino A, Gadda G, Malaguti R, Milano L, Zamboni P. **Development of a plethysmography system for use under microgravity conditions**. Sensors and actuator, 2018; 249-57.

[77] Bruns A. **Fourier-, Hilbert- and wavelet-based signal analysis: are they really different approaches?** Journal of Neuroscience Methods, 2004;137:321–32.

[78] Sifuzzaman M, Islam M R, Ali MZ. **Application of wavelet transform and its advantages compared to Fourier transform**. J Phys Sci, 2009;13:121-34.

[79] Nowak J A, Ocon A, Taneja I, Medow M S, Steward J M. **Multiresolution wavelet analysis of time-dependent physiological responses in syncopal youths**. AM J Physiol Heart Circ Physiol, 2009;296:171-9

[80] Hettmansperger T P, McKean J W. **Robust nonparametric statistical methods**. Kendall's Library of Statistics, 1998.

[81] Jolliffe I T. **Principal Component Analysis** Springer Series in Statistics, 2002;487.

[82] Weisstein E W. **Cross-Correlation**. From MathWorld–A Wolfram Web Resource. http://mathworld.wolfram.com/Cross-Correlation.html

[83] Fawcett T. **An Introduction to ROC Analysis**. Pattern Recognition Letters, 2006;27:861–74.

[84] **GE, LOGIQ S6, Technical Manual**

[85] Kumar P, Clark M. **Medical Management and Therapeutics** Saunders ltd, 2011:555.

[86] Magnano C, Belov P, Krawiecki J, Hagemeier J, Beggs C, Zivadinov R. **Internal Jugular Vein Cross-Sectional Area Enlargement Is Associated with Aging in Healthy Individuals**. PLoS ONE, 2016;11(2):e0149532.

Thanks

Grazie al Professor Mauro Gambaccini, al Professor Paolo Zamboni e al dottor Francesco Sisini dell'Università di Ferrara per avermi dato l'opportunità di svolgere questa bella esperienza di dottorato.

Thanks to Professor Magnus Cinthio and his group of the University of Lund for their kind hospitality in Sweden.

Thanks to Professor Clive Beggs of the University of Leeds for his statistical lessons.

Grazie alla dottoressa Erica Menegatti, alla dottoressa Anna Maria Malagoni e al dottor Mirko Tessari dell'Ospedale Univeristario di Ferrara per il loro prezioso aiuto.

Grazie al dottor Giacomo Gadda e al dottor Adriano Contillo del dipartimento di Fisica e Scienze della Terra dell'Univeristà di Ferrara per i meravigliosi consigli.